AGU PUBLICATIONS

JGR

Journal of Geophysical Research: Atmospheres

RESEARCH ARTICLE
10.1002/2016JD024859

Key Points:
- The VIIRS AOT data coverage was extended to bright and soil-dominated surfaces in the enhanced retrieval algorithm over land
- The VIIRS AOT retrievals from the enhanced algorithm are comparable to that from MODIS Deep Blue algorithm over bright surfaces
- The VIIRS AOT retrievals over dark surfaces from the enhanced algorithm have improved accuracy when compared to the current algorithm

Correspondence to:
H. Zhang,
hai.zhang@noaa.gov

Citation:
Zhang, H., S. Kondragunta, I. Laszlo, H. Liu, L. A. Remer, J. Huang, S. Superczynski, and P. Ciren (2016), An enhanced VIIRS aerosol optical thickness (AOT) retrieval algorithm over land using a global surface reflectance ratio database, *J. Geophys. Res. Atmos.*, *121*, 10,717–10,738, doi:10.1002/2016JD024859.

Received 25 JAN 2016
Accepted 30 AUG 2016
Accepted article online 4 SEP 2016
Published online 17 SEP 2016

An enhanced VIIRS aerosol optical thickness (AOT) retrieval algorithm over land using a global surface reflectance ratio database

Hai Zhang[1], Shobha Kondragunta[2], Istvan Laszlo[2,3], Hongqing Liu[1], Lorraine A. Remer[4], Jingfeng Huang[3], Stephen Superczynski[5], and Pubu Ciren[1]

[1]I. M. Systems Group at NOAA, College Park, Maryland, USA, [2]NOAA NESDIS STAR, College Park, Maryland, USA, [3]University of Maryland College Park, College Park, Maryland, USA, [4]Joint Center for Earth Systems Technology (JCET), University of Maryland Baltimore County, Baltimore, Maryland, USA, [5]Systems Research Group, College Park, Maryland, USA

Abstract The Visible/Infrared Imager Radiometer Suite (VIIRS) on board the Suomi National Polar-orbiting Partnership (S-NPP) satellite has been retrieving aerosol optical thickness (AOT), operationally and globally, over ocean and land since shortly after S-NPP launch in 2011. However, the current operational VIIRS AOT retrieval algorithm over land has two limitations in its assumptions for land surfaces: (1) it only retrieves AOT over the dark surfaces and (2) it assumes that the global surface reflectance ratios between VIIRS bands are constants. In this work, we develop a surface reflectance ratio database over land with a spatial resolution $0.1° \times 0.1°$ using 2 years of VIIRS top of atmosphere reflectances. We enhance the current operational VIIRS AOT retrieval algorithm by applying the surface reflectance ratio database in the algorithm. The enhanced algorithm is able to retrieve AOT over both dark and bright surfaces. Over bright surfaces, the VIIRS AOT retrievals from the enhanced algorithm have a correlation of 0.79, mean bias of −0.008, and standard deviation (STD) of error of 0.139 when compared against the ground-based observations at the global AERONET (Aerosol Robotic Network) sites. Over dark surfaces, the VIIRS AOT retrievals using the surface reflectance ratio database improve the root-mean-square error from 0.150 to 0.123. The use of the surface reflectance ratio database also increases the data coverage of more than 20% over dark surfaces. The AOT retrievals over bright surfaces are comparable to MODIS Deep Blue AOT retrievals.

1. Introduction

Over the past decades, satellites have been providing aerosol data over large spatial and temporal domains [e.g., *Kaufman*, 1987; *Levy et al*., 2007b, 2010; *Kahn et al*., 2005, 2010; *Torres et al*., 2007; *Prados et al*., 2007; *de Leeuw et al*., 2015; *Popp et al*., 2016]. These data are used extensively by the research community to evaluate the impact of aerosols on global and regional climate change [e.g., *Kaufman et al*., 2002; *Bellouin et al*., 2005; *Quaas et al*., 2008]. They are also used to monitor the air quality as an input to models used to estimate PM2.5 (particulate matter with diameter less than 2.5 μm) over broad areas away from surface monitors [e.g., *Engel-Cox et al*., 2004; *Al-Saadi et al*., 2005; *Hoff et al*., 2009; *van Donkelaar et al*., 2010, 2016].

The Visible/Infrared Imager Radiometer Suite (VIIRS) on board the Suomi National Polar-orbiting Partnership satellite, launched in October 2011, supplies multispectral data suitable for quantitative retrieval of aerosol. VIIRS is a scanning radiometer collecting visible and infrared imagery and radiometric measurements. The VIIRS sensor covers the whole globe twice per day, once during the day time and once during the night. However, information on aerosol is retrieved only from daytime observations, obtained at about 1:30 P.M. local time.

The current VIIRS aerosol retrieval algorithm [*Jackson et al*., 2013] retrieves aerosol optical thickness (AOT) over land for dark pixels only. A pixel is determined to be too bright for this dark target algorithm if its top of atmosphere (TOA) reflectance in the 2.25 μm band is greater than 0.3 or the bright pixel index is less than 0.05 [*Godin*, 2015]. The bright pixel index is defined as the short wave infrared normalized difference vegetation index (SWIR NDVI) between VIIRS band M8 (1.24 μm) and band M11 (2.25 μm). However, in this paper, we adopt the definition of a dark pixel from the Moderate Resolution Imaging Spectroradiometer (MODIS) aerosol algorithm such that a pixel is dark if the TOA reflectance in the band 2.25 μm is less than 0.25 [*Levy et al*., 2007b]. The current operational VIIRS aerosol product produces AOT at a 6 km nominal spatial resolution and also at a 750 m nominal spatial resolution [*Liu et al*., 2014].

Table 1. VIIRS Bands Used in AOT Retrieval Over Land

VIIRS Bands	Central Wavelength (μm)
M1	0.412
M2	0.445
M3	0.488
M5	0.672
M11	2.25

Limiting the retrieval of AOT to only dark surfaces leaves large gaps where there are no retrievals, such as the bright desert areas in North Africa and the Arabian Peninsula, etc.

The current operational algorithm uses fixed surface reflectance ratios between different bands in the visible and SWIR ranges of the spectrum [*Jackson et al*., 2013]. The physical reason for this assumption is the simultaneous change of chlorophyll and water in healthy vegetation, and therefore, absorption of visible light by chlorophyll and shortwave infrared radiation by liquid water varies simultaneously [*Kaufman et al*., 2002]. Over a bright surface where there is little or no vegetation coverage, this assumption fails and therefore the algorithm is no longer applicable. Even over dark surfaces, this assumption is not equally accurate everywhere, which can consequently reduce the AOT retrieval accuracies. We will show in the following sections that these ratios are not constant: they are functions of geography and geometry. They are also functions of season in the areas with seasonal change of vegetation colors, but we do not take seasonal variation into consideration in this paper and will investigate seasonality in future research.

In this paper, we enhance the VIIRS aerosol retrieval algorithm over land such that it is able to retrieve AOT over bright surfaces, as well as dark. The approach is similar to that in the current operational VIIRS AOT retrieval algorithm but with some modifications. The enhanced algorithm uses surface reflectance ratios defined between the same channel pairs as in the current dark pixel algorithm with the exception that these new ratios include bright surfaces and are functions of region and geometry.

Below we present the development of the global surface reflectance ratio database using 2 years of VIIRS observations. We apply the database in the VIIRS AOT retrieval algorithm, and we compare the retrieval results with ground observations from AERONET (Aerosol Robotic Network) and those from the MODIS Deep Blue algorithm [*Hsu et al*., 2004, 2006, 2013; *Sayer et al*., 2013].

2. Data

2.1. VIIRS Data

The VIIRS data used in this work include VIIRS level 1B TOA measurements from 16 different M bands (moderate resolution bands), geolocation data, and cloud mask data [*Cao*, 2013a, 2013b; *Godin*, 2014]. The level 1B TOA measurements and geolocation data are also called SDR (Sensor Data Records) data. The spatial resolution of the data is 750 m at nadir. The width of a VIIRS swath is about 3040 km in the cross-track direction. Five bands are used mainly in the AOT retrieval over land, both in the operational algorithm and this work: M1, M2, M3, M5, and M11. The central wavelengths of these bands are shown in Table 1. Several SDR data from the other bands and VIIRS cloud mask data are used for screening, such as clouds, snow ice, etc. We use a 2 year data set (May 2012 to April 2014) in this work.

2.2. AERONET AOT Data

AERONET AOT data are ground measurements of AOT with well-characterized and narrow uncertainty and are generally considered as ground truth to evaluate the performance of satellite AOT retrievals [*Holben et al*., 1998, http://aeronet.gsfc.nasa.gov/]. We use level 1.5 AERONET AOT in this study, since the quality assured that level 2.0 AERONET data were not available for some sites at the time when we performed this research.

3. Current Operational VIIRS AOT Retrieval Algorithm Over Dark Surfaces

The new algorithm developed in this work is an enhancement of the current VIIRS AOT retrieval algorithm over dark surfaces [*Jackson et al*., 2013]. Therefore, we first provide an overview of the present algorithm, before presenting our modifications.

The algorithm retrieves AOT at 0.55 μm from the TOA reflectances of VIIRS bands M1 (0.412 μm), M2 (0.445 μm), M3 (0.488 μm), M5 (0.672 μm), and M11 (2.25 μm), as shown in Table 1. Although AOT is a function

Table 2. VIIRS Surface Reflectance Ratios Used in the Current Operational AOT Retrieval Algorithm Over Land

Band Pairs	Surface Reflectance Ratios
M1/M5	0.513
M2/M5	0.531
M3/M5	0.645
M11/M5	1.788

of wavelengths, those wavelengths are linked by selection of the aerosol model during the retrieval. Once the AOT at 0.55 μm and the aerosol model are determined, AOT at the other wavelength are known automatically. Following the convention of the community, e.g., MODIS AOT, operational VIIRS AOT, GOCART model AOT [*Levy et al*., 2007b; Jackson et al., 2013; *Chin et al*., 2014], the AOT in this work is also reported at 0.55 μm. The retrieval is based on matching predefined, expected surface spectral reflectance ratios M1/M5, M2/M5, M3/M5, and M11/M5 to ones retrieved from VIIRS-observed TOA reflectances by varying the AOT for each of five candidate aerosol models (dust, low-absorption smoke, high-absorption smoke, clean urban, and polluted urban). The aerosol model is selected using different band pairs, and thus, the spectral dependence is a selection criterion. In the VIIRS operational dark pixel algorithm, the surface reflectance ratios between M1 and M5, M2 and M5, M3 and M5, and M11 and M5 are assumed to be constant. Table 2 shows the surface reflectance ratios used in the algorithm.

The algorithm uses a look-up table (LUT) to calculate TOA reflectance or perform atmospheric correction for given conditions. The LUT stores precalculated components in the radiative transfer equation using the 6S radiative transfer model [*Vermote et al*., 1997; *Kotchenova et al*., 2006; *Kotchenova and Vermote*, 2007] for different aerosol models, different geometries, and different VIIRS bands [*Godin*, 2015]. The LUT contains calculations for five aerosol models: dust (spherical), high-absorption smoke, low-absorption smoke, clean urban, and polluted urban models, as shown in Table 3.

The algorithm only performs AOT retrieval for sunlit pixels without cloud, without snow ice, and without fire through the use of VIIRS cloud product and internal tests [*Godin*, 2014, 2015]. If a pixel satisfies these conditions, the algorithm continues to retrieve AOT, shown in Figure 1 with red boxes. The blue boxes represent the algorithm modifications in this work, which will be described in section 6. For each VIIRS pixel, the algorithm loops over different aerosol models and AOT to find the best match such that the aerosol model and the AOT pair gives the lowest residual between the retrieved surface reflectances and those calculated from

Table 3. The Microphysical Properties of the Aerosol Models Used in the Current VIIRS Dark Target Algorithm (Spherical Dust, Low-Absorption Smoke, High-Absorption Smoke, Clean Urban, Polluted Urban; [*Jackson et al*., 2013; *Godin*, 2015]) and the Enhanced Algorithm (Spheroid Dust, Low-Absorption Smoke, High-Absorption Smoke, Clean Urban, Polluted Urban)[a]

	Dust (Spherical)	Smoke, Low Absorption	Smoke, High Absorption	Urban, Clean	Urban, Polluted	Dust (Spheroid)
			Refractive Indices			
Real part	1.48	1.47	1.51	$1.41–0.03\tau_{0.44}$	1.47	$1.48\tau^{-0.021}$, $1.48\tau^{-0.021}$, $1.48\,\tau^{-0.021}$,$1.46\,\tau^{-0.040}$ [c]
Imaginary part	-[b]	0.0093	0.021	0.003	0.014	$-0.0025\tau^{0.132}$, -0.002, $-0.0018\tau^{-0.08}$, $-0.0018\tau^{-0.30}$ [c]
			Size Parameter Fine Mode			
Volume mean radius (μm)	0.12	$0.13+0.04\tau_{0.44}$	$0.12+0.025\tau_{0.44}$	$0.12+0.11\tau_{0.44}$	$0.12+0.04\tau_{0.44}$	$0.1416\tau^{-0.052}$
Standard deviation	$0.49+0.10\tau_{1.02}$	0.40	0.40	0.38	0.43	$0.7561\tau^{0.148}$
Volume concentration ($\mu m^3/\mu m^2$)	$0.02+0.02\,\tau_{1.02}$	$0.12\,\tau_{0.44}$	$0.12\,\tau_{0.44}$	$0.15\,\tau_{0.44}$	$0.12\,\tau_{0.44}$	$0.0871\tau^{1.026}$
			Size Parameter Coarse Mode			
Volume mean (μm)	1.90	$3.27+0.58\,\tau_{0.44}$	$3.22+0.71\,\tau_{0.44}$	$3.03+0.49\,\tau_{0.44}$	$2.72+0.60\,\tau_{0.44}$	2.2
Standard deviation	$0.63–0.10\,\tau_{1.02}$	0.79	0.73	0.75	0.63	$0.554\tau^{-0.052}$
Volume concentration ($\mu m^3/\mu m^2$)	$0.9\,\tau_{1.02}$	$0.05\,\tau_{0.44}$	$0.09\,\tau_{0.44}$	$0.01+0.04\,\tau_{0.44}$	$0.11\,\tau_{0.44}$	$0.6786\tau^{1.057}$

[a]The spheroid dust model is obtained from MODIS aerosol algorithm [*Levy et al*., 2007a]; $\tau_{0.44}$, τ, and $\tau_{1.02}$ are AOTs at wavelengths 0.44, 0.55, and 1.02 μm, respectively.

[b]The imaginary part of the index of refraction for dust (spherical) is defined for the following (wavelength, index of refraction) pairs: (0.350 μm, 0.0025), (0.400 μm, 0.0025), (0.412 μm, 0.0025), (0.443 μm, 0.0025), (0.470 μm, 0.0023), (0.488 μm, 0.0021), (0.515 μm, 0.0019), (0.550 μm, 0.0016), (0.590 μm, 0.0013), (0.633 μm, 0.0010), (0.670 μm, 0.0007), (0.694 μm, 0.0007), (0.760 μm, 0.0007), (0.860 μm, 0.0006), (1.240 μm, 0.0006), (1.536 μm, 0.0006), (1.650 μm, 0.0006), (1.950 μm, 0.0006), (2.250 μm, 0.0006) and (3.750 μm, 0.0006).

[c]The four values represent reflective index at four wavelengths: 0.47, 0.55, 0.66, and 2.1 μm, respectively.

surface reflectance ratios with M5. To do this, for each aerosol model of the five models in the LUT, starting from the lowest AOT in the LUT, the algorithm computes the corrected reflectance from the measured TOA reflectance of bands M3 and M5 through atmospheric correction. The algorithm calculates the difference between atmospherically corrected reflectance predicted from M5 through the ratio and the atmospherically corrected reflectance in M3, i.e., $\Delta\rho_3(\tau) = \rho_3(\tau) - R_3\rho_5(\tau)$, where R_3 is the predefined surface reflectance ratio between M3 and M5, $\rho_3(\tau)$ and $\rho_5(\tau)$ are atmospherically corrected reflectance using AOT value τ. If the value $\Delta\rho_3$ is greater than 0, the algorithm increases AOT and repeats the process until this value is less than 0. Then, the algorithm obtains the AOT that gives the difference 0 through interpolation between the two consecutive AOT values that give positive and negative atmospherically corrected reflectance difference $\Delta\rho_3$. There are totally five different AOT values for the five aerosol models in the LUT.

The final aerosol model is chosen from the five predefined aerosol models such that it gives the minimum residual for the surface reflectances of the other channels, i.e., M1, M2, M11, defined as

$$\text{residual} = \sum_i \left(\rho_{\text{sfc},i} - R_i\rho_{\text{sfc},5}\right)^2, \tag{1}$$

where i represents band number, $\rho_{\text{sfc},i}$ is the surface reflectance at band i obtained by atmospheric correction using the AOT obtained through M3/M5, and R_i is the surface reflectance ratio between band i (Mi) and M5.

The predefined surface reflectance ratio of M3/M5 affects the AOT retrieved. In areas where the actual M3/M5 ratio is larger than the one used in the algorithm, the retrieved AOT will be underestimated, and where the actual ratio is smaller, AOT will be overestimated. Thus, the accuracy of the VIIRS AOT retrieval over land is strongly dependent on the predefined M3/M5 ratio. This is the reason why the current VIIRS algorithm is applied only to dark surface targets. Uncertainty in aerosol retrievals is dependent on the uncertainty in estimated surface reflectance. Roughly, an error of 0.01 in estimated surface reflectance translates into an error of 0.10 in retrieved AOT, while an error of 0.02 in surface reflectance translates into an AOT error of 0.20, etc [*Kaufman et al*., 1997a, 1997b]. However, the translation of uncertainty from estimated ratio to surface reflectance is dependent on the absolute surface reflectance and, therefore, darker surfaces will have smaller uncertainties than brighter ones. For example, in *Jackson et al*. [2013], the global M3/M5 ratio is given as 0.645 ± 0.079, where the uncertainty range is 1 standard deviation. If we apply the uncertainties in the global M3/M5 ratio (±0.079) to a dark surface of $\rho_{\text{sfc}} = 0.05$ in band M5, the range of uncertainty in surface reflectance is approximately ±0.004, which translates into AOT uncertainty of ±0.04. However, if we apply the same uncertainty in ratio to a bright surface of $\rho_{\text{sfc}} = 0.35$ in band M5, the uncertainty in surface reflectance is ±0.027 and the resulting AOT uncertainty is ±0.27. In order to retrieve AOT over brighter surfaces with sufficient mean bias and standard deviation of error, the error bars in the surface reflectance ratios must be narrowed considerably.

In addition to the screening mentioned above, i.e., cloud, snow ice, and fire, the algorithm also performs the following screening for quality control: cloud adjacency, cloud shadow, invalid SDR data, cirrus, solar zenith angle range check, and AOT out of range. AOT retrievals over such pixels are either not produced or of degraded quality. Details of these screening can be found in the VIIRS Aerosol Algorithm Theoretical Basis Document [*Godin*, 2015].

4. Extending the AOT Retrieval Algorithm to Bright Surfaces

The main purpose of this work is to enhance the VIIRS retrieval algorithm over land such that the algorithm can retrieve AOT for bright surfaces. The algorithm in this work is similar to the VIIRS dark pixel algorithm as introduced in the previous section [*Jackson et al*., 2013]. For AOT retrieval over bright surfaces, we can follow the same approach if the surface reflectances between the bands used in the retrieval algorithm are well correlated. However, it is not appropriate to use the same fixed global surface reflectance ratios as those in the dark surface algorithm. As mentioned in section 1, those ratios for dark vegetated surfaces will not be the same for bright surfaces of desert or bare soil. Furthermore, errors in surface reflectance estimates over these brighter surfaces enhance the propagation of error to the AOT, as explained above. The surface reflectance ratios between different bands are determined by the composition of different surface types, since different compositions reflect the sunlight differently in different spectral ranges; i.e., they have different colors. Therefore, they should be different from those over the dark vegetated surfaces.

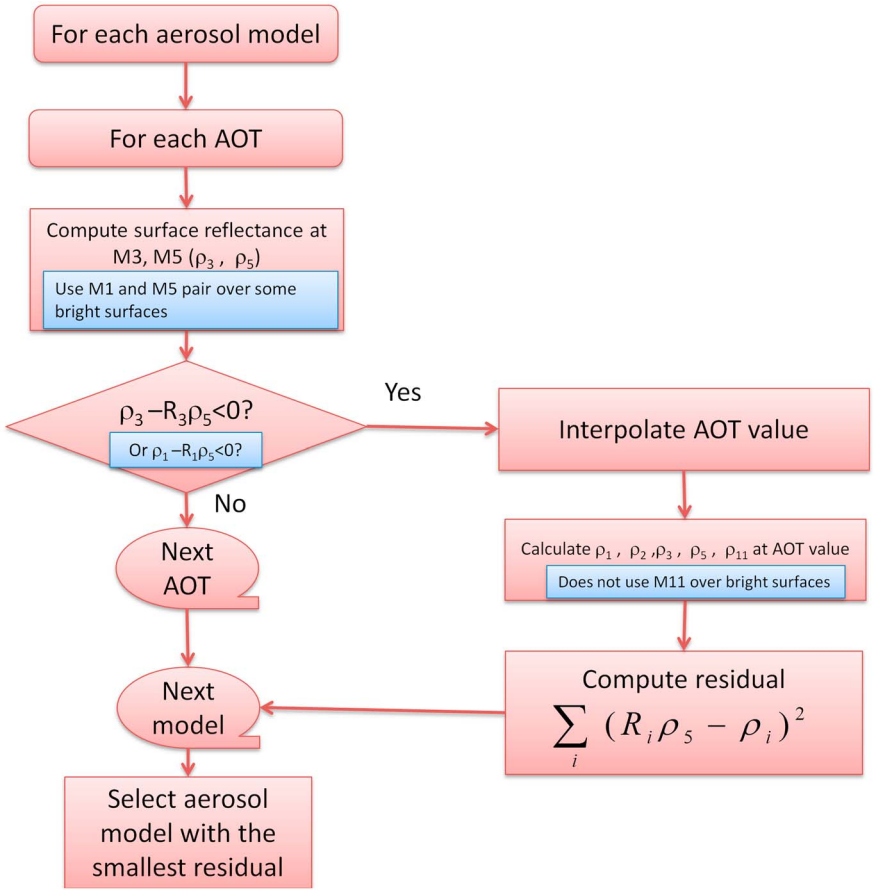

Figure 1. Flow chart of the current operational AOT retrieval algorithm (in red boxes) and the modifications (in light blue boxes).

In a global algorithm specific band ratios cannot be determined and applied for every individual 750 m pixel, due to the limitation of computational resources. Instead, we will use fixed surface reflectance ratios over small regions, when the correlations of the surface reflectance between different bands are high, as will be demonstrated in the following paragraphs using the VIIRS and AERONET data at Solar Village and Banizoumbou AERONET sites.

To determine the surface reflectance from the TOA measurements at the AERONET sites of Solar Village and Banizoumbou, we make an atmospheric correction for all VIIRS-AERONET collocations (matchups) using the measured AOT from AERONET, ancillary data such as surface pressure and LUT. The structure of the LUT is the same as that used in the operational VIIRS AOT retrieval algorithm as described above [*Jackson et al.*, 2013]. However, we substitute the spheroid dust model used in MODIS [*Levy et al.*, 2007b] in the LUT (the last column in Table 3), while the operational VIIRS LUT uses a spherical dust model. The other four aerosol models are the same as the ones used in the operational VIIRS aerosol algorithm over land. We also extend the maximum AOT to 5.0 by adding one more AOT value in the LUT, while the maximum AOT in the operational VIIRS algorithm is 2.0.

Atmospheric correction is applied to each VIIRS pixel within 10 km of the AERONET station for each VIIRS band. Figures 2 and 3 show the scatterplots of bands M1, M2, M3, and M11 versus M5 surface reflectance on two selected days, which have low AERONET AOT (0.04 and 0.06 as shown in the captions of the figures) so that the atmospheric correction is the least affected by the choice of the aerosol models. The aerosol model used in the atmospheric correction is the dust model, since these two sites are located in the deserts and we assume that dust model is the most often observed aerosol model.

From the scatter plots, we can see that the surface reflectances in bands M1, M2, M3, and M11 all have relatively good correlation with the surface reflectance in band M5. Therefore, we can potentially use these ratios

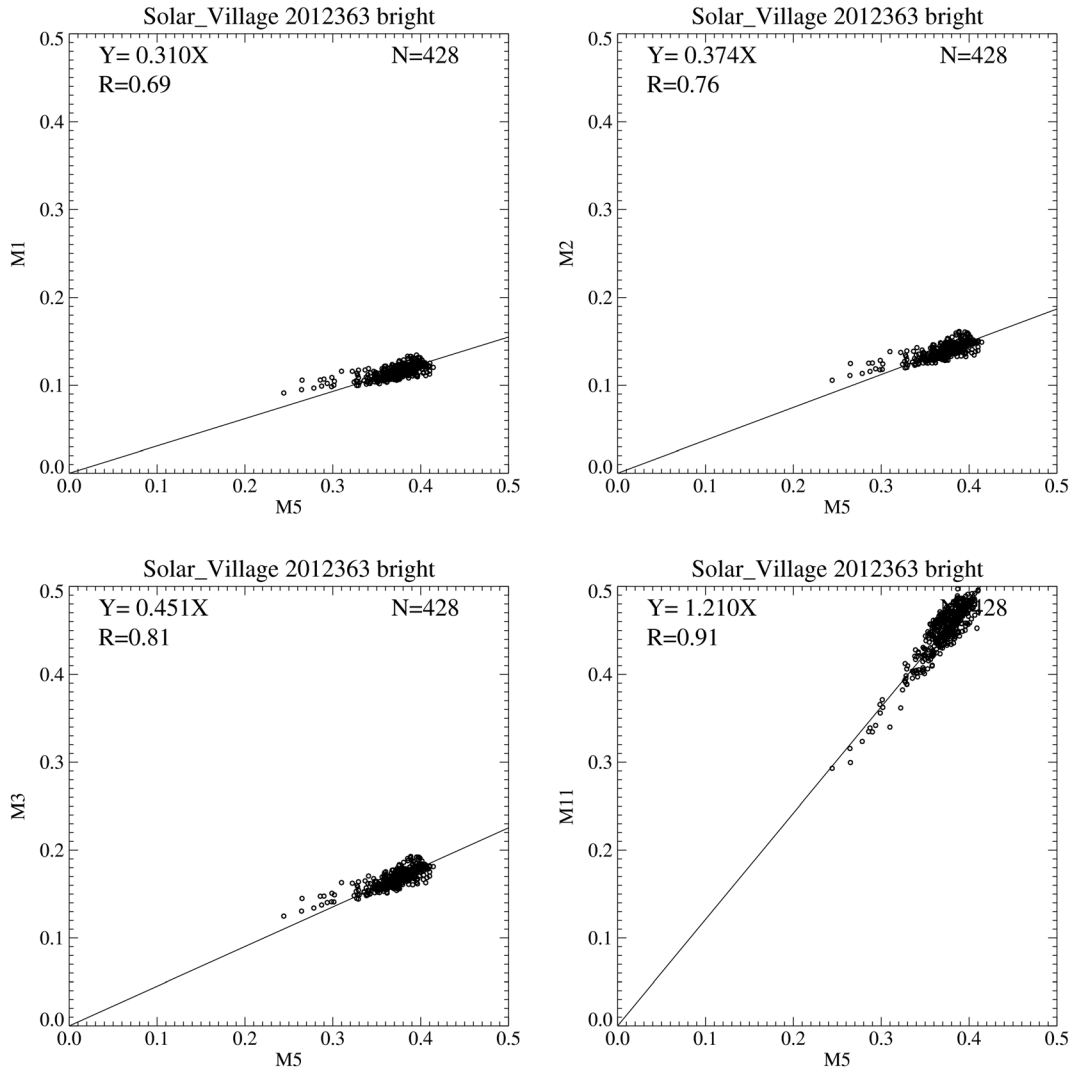

Figure 2. Scatterplots of atmospheric corrected surface reflectance between different bands and band M5 at Solar Village AERONET site on 28 December 2012. The matchup AERONET AOT of 0.04 was used for the atmospheric correction. Only bright pixels are selected, defined as TOA reflectance of M11 greater than 0.25. The regression line is obtained through least squares fit and is forced to pass through the origin.

to retrieve AOT over bright surfaces with a similar algorithm as the dark surface algorithm. Over bright surfaces, surface reflectance of both M5 and M11 are close to the critical reflectance (the surface reflectance at which TOA reflectance does not change with respect to the change of aerosol load) and their TOA reflectance are not affected much by aerosols, because the contribution of the aerosol scattering and absorption tends to cancel each other [*Fraser and Kaufman*, 1985]. Since the M5 and M11 bands have limited sensitivity to aerosol over bright surfaces, the M11/M5 ratio will not add information to the aerosol retrieval. Therefore, we do not use M11 in the retrieval algorithm over bright surfaces. The surface reflectance ratios at the two sites differ from each other, and they are also different from those used in the operational dark pixel algorithm, shown in Table 2. For example, the M3/M5 ratio is 0.451 at Solar Village, 0.392 at Banizoumbou, and 0.645 in the operational dark pixel algorithm. Consequently, we cannot expect to achieve a good AOT retrieval if we use a fixed value for all locations, globally. Instead, we must develop a global surface reflectance ratio database for all retrieval locations.

An alternative way to estimate surface reflectance is by using the average surface reflectance over a small region. Table 4 shows a comparison of the RMSE of estimated surface reflectance for these VIIRS pixels in the above examples using two methods: (1) estimate the surface reflectance using average surface reflectance

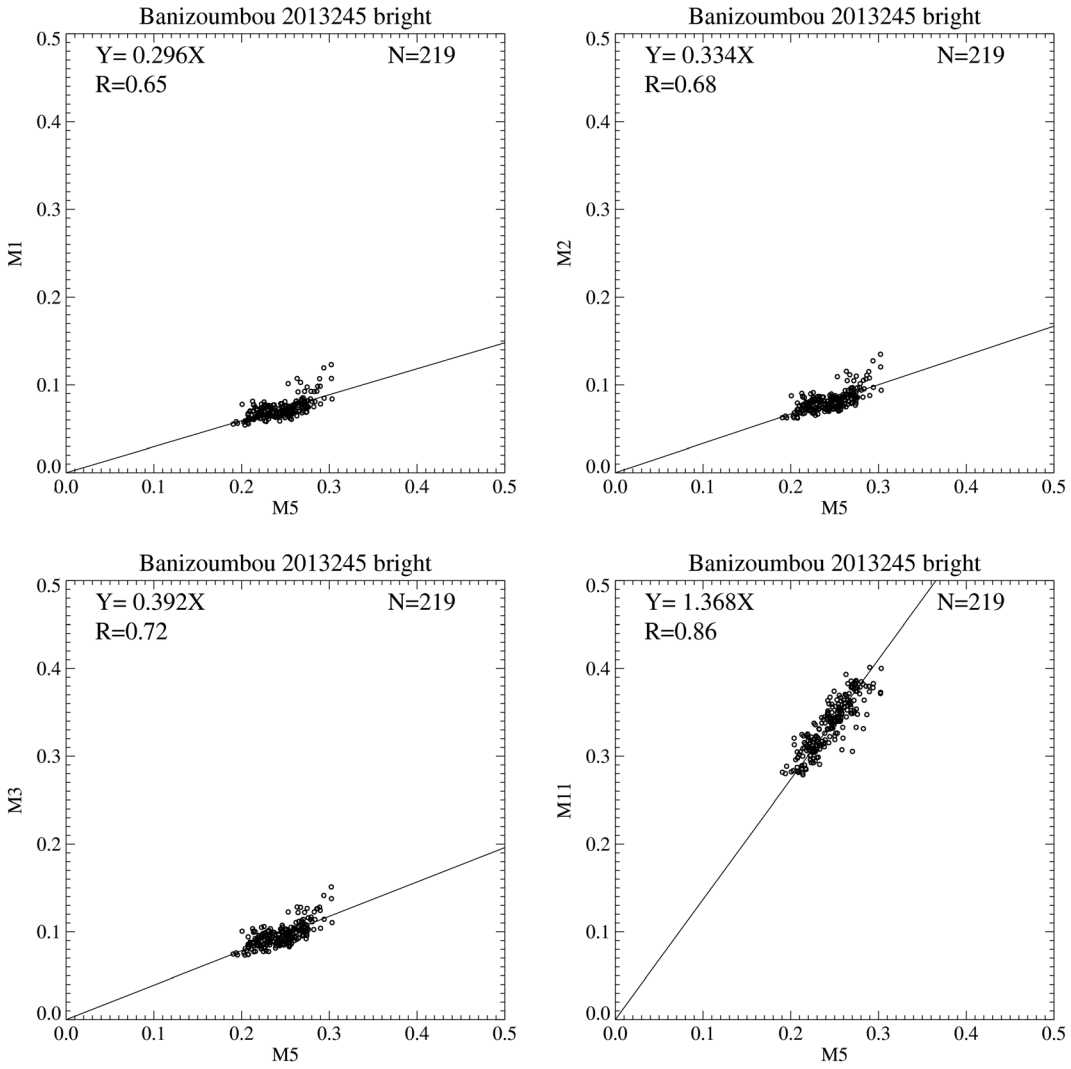

Figure 3. Same as Figure 2 but for Banizoumbou on 2 September 2013. The matchup AERONET AOT is 0.06, which was used in the atmospheric correction.

and (2) estimate the surface reflectance using the ratios between bands M1, M2, M3, and M5. The RMSE is smaller for all the three bands in the two cases if the second method is used. One of the reasons that the ratios are more stable than the absolute reflectance is because of the variation in scene brightness resulting from topography. The use of ratios to minimize topographic and scene brightness effect has been used in the Landsat image processing [e.g., *Schowengerdt*, 1983].

First, we question how representative these 2 days are at Solar Village and Banizoumbou: How much variability is there in surface reflectance ratio in an analysis applied over the span of 2 years of matchups between VIIRS and AERONET? To answer this question, we performed atmospheric correction on the AERONET matchup data set at these two sites using the AERONET AOT and the dust aerosol model described above, since the aerosols at the two sites are dominated by dust [*Dubovik et al*., 2002; *Holben et al*., 1998]. For each observation, we derived the surface reflectance ratio between M1 and M5, M2 and M5, and M3 and M5 when the number of cloud-free pixels was greater than 50 over the 10 km radius around the site. The surface reflectance ratios were then determined through averaging the ratios at each observation of the matchup data set at each site. The average surface reflectance ratios and the standard deviations are shown in Table 5. The variability in surface reflectance ratio at Solar Village is only 30% of the variability at Banizoumbou in an absolute sense and even less in a relative sense. Besides the surface surrounding Solar Village being more uniform, we also note that Banizoumbou has a smoke season in addition to the dust that dominates year-round

Table 4. Comparison of RMSE of the Surface Reflectance Estimates Two Methods for the Two Cases at Solar Village and Banizoumbou in Figures 2 and 3: (1) Using Average Surface Reflectance Within 10 km; (2) Using Ratios Between the Bands and M5 Band

	Solar Village			Banizoumbou		
Bands	RMSE Using Average Surface Reflectance	RMSE Using Ratios With M5	Average Surface Reflectance	RMSE Using Average Surface Reflectance	RMSE Using Ratios With M5	Average Surface Reflectance
M1	0.007	0.005	0.115	0.010	0.008	0.072
M2	0.008	0.006	0.140	0.011	0.008	0.081
M3	0.010	0.006	0.168	0.012	0.008	0.096

[*Cavalieri et al*., 2010]. The smoke may introduce inaccuracy into the atmospheric correction, which would introduce greater variability in the derived surface reflectance ratios and contribute to greater uncertainty ultimately in the retrieval of AOT.

How accurately can we retrieve AOT at these sites, given the new derived surface reflectance ratios? Next, we retrieve AOT using one of the three (M1/M5, M2/M5, and M3/M5) surface reflectance ratios with the dust model. Note that here we are assuming that a single value of surface ratio can be used by all pixels within 10 km of the station to retrieve the AOT. The algorithm is the same as the VIIRS operational AOT retrieval algorithm in that it looks for the AOT value that makes the atmospherically corrected reflectance ratio equal to the predefined ratio. We compare the AOT retrieval results against AERONET AOT and show the scatterplots in Figure 4. The scatterplots demonstrate that we can use any of these three surface reflectance ratios for the AOT retrieval with only slightly different statistics with respect to AERONET AOT.

To evaluate the uncertainty of the AOT retrieval due to the uncertainty of the surface reflectance ratios, we simulate the AOT retrieval using the surface reflectance, ratios, and standard deviation shown in Tables 4 and 5. We first do forward calculations using an input AOT = 0.6, dust model, and surface reflectances shown in Table 3 for eight example geometries (as shown in Table 6), following those in Table 3 in *Levy et al*. [2007b]. The calculated TOA reflectances are then fed to the AOT retrieval algorithm using different band pairs. AOT is retrieved using different pairs of ratios, i.e., M1/M5, M2/M5, or M3/M5, which are perturbed by the standard deviation in Table 5. From this simulation, we found that the AOT retrieved have errors of about 0.11 at Solar Village and 0.19 at Banizoumbou. If we use the ratios in the current operational algorithm for AOT retrieval instead, we do not retrieve any positive AOT retrievals for any of the cases.

This exercise demonstrates that the AOT can be retrieved over bright surfaces with reasonable accuracy if we have good estimates of the surface reflectance ratios and that a single value of surface ratio can be used to represent a region on the order of 10 km. The better the estimate of the ratios, the more accurate the AOT retrieval, although the benefit of better ratio estimates is not linear. While the estimate of ratio at Solar Village is at least 4 times better than at Banizoumbou, the resulting AOT retrieval at Solar Village is not even twice as accurate. It also serves as an estimate of expected performance under "ideal" conditions. Still there is scatter, likely tied to the influence of seasonality of both surface conditions and aerosol type, and also geometry.

5. Surface Reflectance Ratio Database

As demonstrated in the previous section, the surface reflectance ratios are different at different locations. In this section, we describe the method to build a global surface reflectance ratio database for the enhanced AOT retrieval algorithm. In the previous section we showed that a single value representing the surface reflectance ratio of a 10 km area around the AERONET station could produce reasonable AOT retrievals. Therefore,

Table 5. Surface Reflectance Ratios at the Two African AERONET Sites

	Solar Village			Banizoumbou		
Band Pairs	Sample Size	Mean	Standard Deviation	Sample Size	Mean	Standard Deviation
M1/M5	384	0.296	0.028	326	0.207	0.068
M2/M5		0.370	0.019		0.275	0.057
M3/M5		0.456	0.014		0.359	0.047

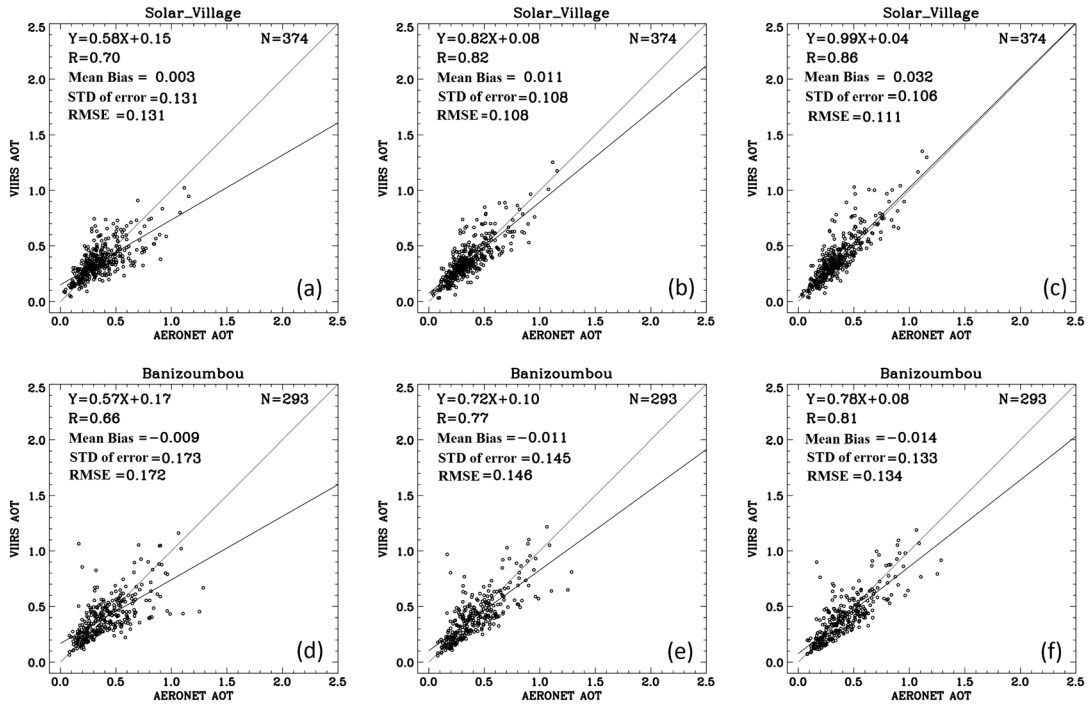

Figure 4. Scatterplots of VIIRS AOT retrievals versus AERONET AOT at (a–c) Solar Village and (d–f) Banizoumbou using different surface reflectance ratios: M1/M5 for column 1 (Figures 4a and 4d), M2/M5 for column 2 (Figures 4b and 4e), and M3/M5 for column 3 (Figures 4c and 4f).

we assign the spatial resolution of the surface reflectance ratio database as 0.1° × 0.1°, which is basically the same scale. To derive surface reflectance ratios, correcting for Rayleigh scattering and gas absorption is insufficient because of aerosols, even when searching for minimum TOA reflectances in the VIIRS observations over the duration of the 2 year data set. This became apparent when M1 and M5, M2 and M5, M3 and M5, and M5 and M11 ratios increased with increasing AOT, because the TOA reflectances in different bands have different sensitivity to the AOT load. Instead, we assume a background AOT (specified below) to perform atmospheric correction of the TOA reflectance in different bands and calculate the corrected reflectance ratios. The lower bounds of these ratios are used as estimates of the corresponding surface reflectance ratios if we assume that the surface reflectance ratios do not change over seasons. The background AOT is close to 0 over clean areas, as will be shown in section 5.1, and thus does not have much effect on the estimates of the surface reflectance ratios if we simply assume a zero background AOT. However, the background AOT should be taken into account for the atmospheric correction in the areas with either heavy dust or heavy pollutions, such as North Africa, Arabian Peninsula, India, China, etc.

5.1. Background AOT

To estimate the background AOT at each 0.1° × 0.1° box, we start with the global AERONET sites: for each AERONET site over the 2 year period of the study, i.e., May 2012 to April 2014, we use the lowest 5th percentile

Table 6. Solar Satellite Geometries for Eight Examples (Units Are in Degrees)[a]

Reference	Solar Zenith	View Zenith	Relative Azimuth	Scattering Angle
A	12.00	6.97	60.00	163.40
B	12.00	52.84	60.00	120.53
C	12.00	6.97	120.00	169.59
D	12.00	52.84	120.00	132.35
E	36.00	6.97	60.00	140.12
F	36.00	52.84	60.00	104.74
G	36.00	6.97	120.00	147.00
H	36.00	52.84	120.00	136.29

[a]Table 3 in *Levy et al.* [2007b].

Table 7. Bias and RMSE of the Estimated Background AOT With Various Parameter of d_0 in the Weight of the Spatial Kriging Interpolation[a]

d_0 (km)	Bias (Estimated-Measured)	RMSE
100	0.002	0.046
200	0.0007	0.040
500	0.0006	0.039
1000	0.0003	0.041

[a]The global mean background AOT at the AERONET sites is 0.054.

AOT as the estimate of the background AOT. Then we use a method similar to inverse distance weighting [e.g., *Isaaks and Srivastava*, 1989] to interpolate the background AOT across the globe. The background AOT at a location can be estimated as

$$\tau_{\mathrm{int},b}(\mathrm{lat},\mathrm{lon}) = \sum_i w_i \tau_{\mathrm{eb},i} / \sum_i w_i, \quad (2)$$

where $\tau_{\mathrm{int},b}$(lat,lon) represents the interpolated background AOT at location (lat,lon), $\tau_{\mathrm{eb},i}$ represents the estimated background AOT at AERONET site i, w_i represents the weight of the background AOT at site i on the location (lat,lon). We can have many choices for the weight, which should gradually decrease with respect to the distance from the AERONET site. We found that one choice works well, which is defined as $w_i(\mathrm{lat},\mathrm{lon}) = e^{-d_i(\mathrm{lat},\mathrm{lon})/d_0}$, where d_i(lat, lon) represents the distance between AERONET site i and location (lat,lon), and d_0 is a constant. This weight corresponds to an assumption that the representativeness of background AOT from a nearby AERONET site decreases exponentially with distance.

To evaluate the error of this method, we calculate the bias and RMSE as$\mathrm{Bias} = \frac{1}{N}\sum_i \left(\tau_{\mathrm{int},b,i} - \tau_{\mathrm{eb},i}\right)$ and RMSE $= \sqrt{\frac{1}{N}\sum_i \left(\tau_{\mathrm{int},b,i} - \tau_{\mathrm{eb},i}\right)^2}$, where N represents the total number of the AERONET sites, $\tau_{\mathrm{int},b,i}$ is the interpolated background AOT at site i using the data from all the sites except site i. The results with different choices of the parameter d_0 are shown in Table 7. The results show that the change of d_0 does not have significant influence on the derived background AOT: the biases are close to 0 and the RMSEs are around 0.04, with the global mean background AOT at the AERONET sites is 0.054. In this work, we choose $d_0 = 500$ km.

Figure 5 shows the background AOT derived from the AERONET AOT using the above method. The 5th percentiles of AERONET AOT at each AERONET site are also plotted. We can see that the areas with high background AOT are mostly located in India, Arabian Peninsula, North Africa, and China, where heavy pollution or dust are expected. The background AOT can be as high as 0.15 in these regions. The other regions have low background AOT, mostly below 0.05. Seasonally varying background AOT will introduce uncertainty in this method. The difference between the AERONET 5th percentile AOT and the interpolated background AOT indicates the magnitude of the uncertainty in background AOT using this method. With higher uncertainty in background AOT, the uncertainty of the estimated surface reflectance ratio is also higher and therefore influences the retrieved AOT. In general, background AOT uncertainty propagates to the uncertainty of the retrieved AOT with the same magnitude. For example, if we have an uncertainty of 0.1 in background AOT, we expect an uncertainty of 0.1 in retrieved AOT. The background AOT over ocean may be less trustworthy since we have very sparse AERONET sites there. However, it is not used in this work since the AOT retrieval algorithm is designed for and will only be implemented in areas over land.

5.2. Geometry Dependency of Surface Reflectance Ratios

Surface reflectance is usually not Lambertian. Its value is a function of solar zenith angle, satellite zenith angle, and corresponding azimuth angles. The geometry dependence of the surface reflectance is described by the bidirectional reflectance distribution function (BRDF). For example, the MODIS surface albedo product MCD43 represents surface BRDF using a kernel-driven semiempirical BRDF model [*Lucht et al.*, 2000].

Unless BRDFs from different bands have the same shape, the surface reflectance ratios should also be functions of geometries between the satellite and the Sun. For example, in the MODIS AOT retrieval algorithm, the surface reflectance relationship between visible bands and the SWIR band at 2.12 μm is found to be a function of geometry [*Levy et al.*, 2007b; *Remer et al.*, 2001], and it is represented as a function of scattering angle [*Levy et al.*, 2007b].

Although we do not find significant dependence of the surface reflectance ratio on the geometry at the above two AERONET sites, i.e., Solar Village and Banizoumbou, we notice such dependence at some sites in other locations. One example is the Sevilleta site in the western U.S. To demonstrate the dependence of surface reflectance ratios on the scattering angle, we made atmospheric correction on TOA reflectance at

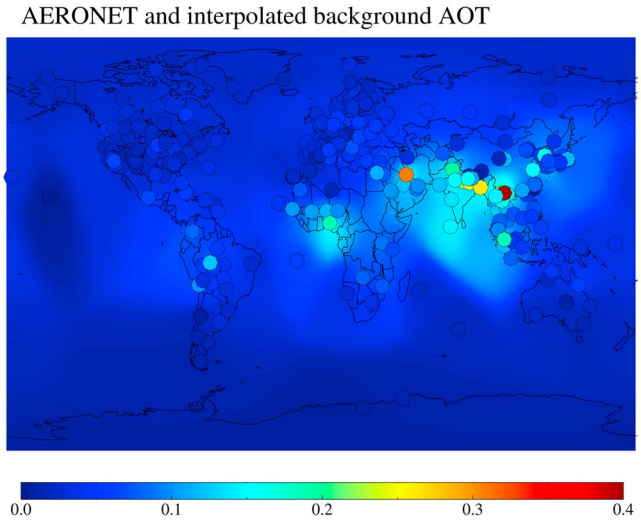

Figure 5. Background AOT derived from 2 year AERONET AOT and interpolated to the other locations.

the Sevilleta site. The TOA reflectance was corrected for the pixels within 10 km of the site with background AOT obtained as above, which is about 0.05. We use the five aerosol models in the LUT to do the atmospheric correction and average the corrected reflectance. For each observation time, the atmospherically corrected reflectance ratios, e.g., M1/M5, M2/M5, etc, were derived for these pixels through linear regression and the regression lines were forced to pass through the origin. In Figure 6, the derived ratios of M1/M5 and M3/M5 were plotted as a function of scattering angle. The ratios were also separated into groups of forward and backward reflection geometry. Forward and backward geometries are defined as follows: if the relative azimuth angle is greater than or equal to 90°, it is called forward reflection geometry; otherwise, it is called backward reflection geometry. The lower bounds of the dots are expected to be close to the corresponding surface reflectance ratios.

To derive the lower bound of the atmospherically corrected ratios, we separated these ratios into bins with a scattering angle width of 10°. In each bin, we look for the lowest 10th percentile of the ratios. This method is similar to averaging the ratios between the minimum and the lowest 20th percentile. However, if there are outliers, the averaging method tends be influenced significantly by them. The choice of the lowest 10th percentile can eliminate the influence of the outliers as long as the outlying points make up less than 10% of the sample. The lower bound lines are derived through a linear regression of these lowest 10th percentile ratios, as shown in the blue (forward) and red (backward) lines in Figure 6. The blue lines and the red lines are not horizontal, indicating dependence of the ratios on the scattering angle. If we used geometry-independent ratios such as the 10th percentile of all the background atmospherically corrected ratios (orange line in Figure 6), we would introduce large errors in some geometries.

We analyze the AOT retrieval errors due to using constant surface reflectance ratios when in reality the ratios could be varying as a function of viewing geometry. We first perform a forward calculation using a surface reflectance at M5 of 0.2 and surface reflectance ratios of M1/M5 = 0.344 and M3/M5 = 0.514, which are the values obtained at the Sevilleta site. The surface reflectance ratios are then perturbed by the variations

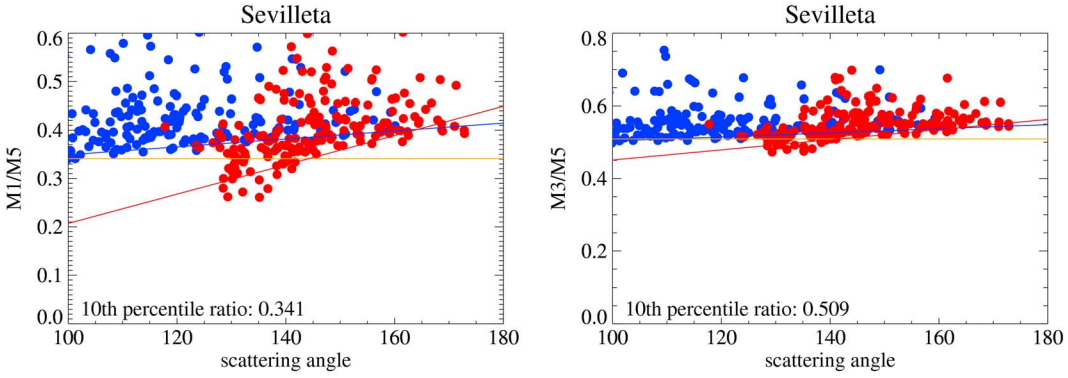

Figure 6. Atmospherically corrected reflectance ratios of (left) M1/M5 and (right) M3/M5 as a function of scattering angle at Sevilleta. Red dots represent ratios in backward geometries, while blue dots represent ratios in forward geometries. The lower bounds are plotted as red and blue lines. The horizontal orange lines represent the 10th percentile of all the points.

Table 8. AOT Retrieval Errors Due To the Different Surface Reflectance Ratios in Different Geometries

	M1/M5 = 0.293 Retrieved AOT		M3/M5 = 0.491 Retrieved AOT		M1/M5 = 0.391 Retrieved AOT		M3/M5 = 0.537 Retrieved AOT	
Input AOT	Range	Mean	Range	Mean	Range	Mean	Range	Mean
0.1	0.14–0.41	0.22	0.13–0.36	0.19	−0.1–0.04	−0.01	−0.07–0.05	0.007
0.4	0.44–0.82	0.54	0.43–0.73	0.50	0.05–0.35	0.25	0.08–0.36	0.29
1.0	1.05–1.33	1.16	1.03–1.20	1.08	0.32–0.94	0.78	0.46–0.96	0.85

due to the differences in different geometries, which are 0.051 and 0.023, respectively. We use these perturbed surface reflectance ratios to retrieve AOT using the same aerosol model that was used in the forward calculation. The procedure is repeated for the different geometries defined in Table 6, and for five different aerosol models and for three different input AOT values (0.1, 0.4, and 1.0). The results are shown in Table 8. We can see that the average uncertainty is in the range of 0.1–0.2, while in some extreme cases it can be as high as 0.6.

5.3. Global Surface Reflectance Ratio Database Derivation

The flowchart in Figure 7 summarizes the procedure to derive global surface reflectance ratios. We divide the globe into 0.1° × 0.1° grid boxes and derive surface reflectance ratios in each grid box using the procedure similar to the one shown above for the Sevilleta AERONET site. We assume that the surface reflectance ratios are different for dark and bright pixels. Therefore, we derive the surface reflectance ratios separately for the two types of pixels. A pixel is defined as a bright pixel if the TOA reflectance of band M11 (2.2 μm) is greater than or equal to 0.25. Otherwise, it is defined as a dark pixel. Since both dark and bright pixels can exist in some grid boxes, we may have two sets of surface reflectance ratios there, i.e., one for the dark pixels and the other for the bright pixels. Because we do not plan to use M11 over bright surfaces, we do not derive surface reflectance ratios of M5/M11 for bright pixels. We use the 2 year VIIRS data set (May 2012 to April 2014) to derive the surface reflectance ratio database. The aerosol models used are based on the geographical regions: dust model over North Africa and the Arabian Peninsula and all five aerosol models in the LUT over the other regions. In the areas that use all the models, the final corrected reflectance ratios are obtained by averaging the five individual ones. The selection of the dust model over North Africa and Arabian Peninsula is because it is the dominant model there [*Dubovik et al.*, 2002].

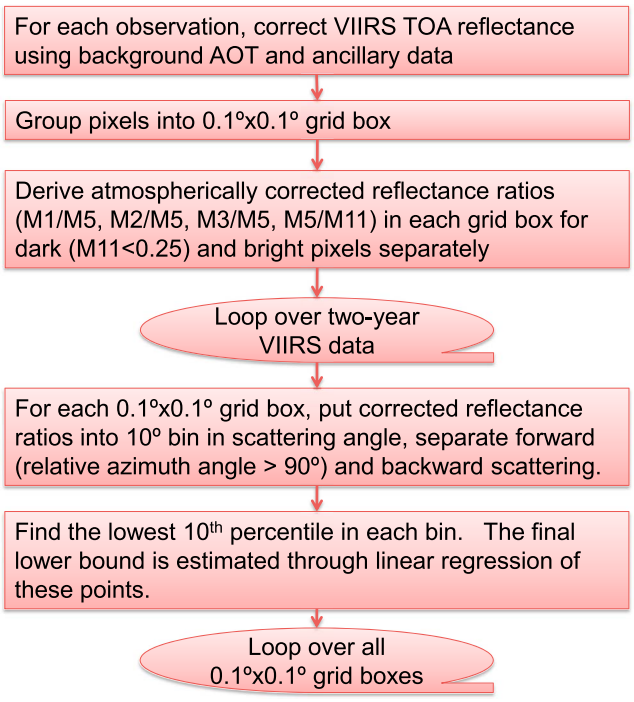

Figure 7. Flowchart for deriving the surface reflectance ratio database.

The choice of aerosol model can affect the derived surface reflectance ratios. To evaluate the uncertainty caused by aerosol model assumption, we perform an analysis using the same geometry settings in Table 6 and the surface reflectance derived in the case study at Solar Village in section 4. As shown in Figure 5, the maximum background AOT is about 0.15. Therefore, in the forward simulation, we use AOT of 0.15 and one of the aerosol models in the LUT to calculate TOA reflectance. In the atmospheric correction, we use the two methods to derive surface reflectance ratios: (1) the ratios from the dust model and 0.15 AOT; (2) average of the ratios derived from each of the five models and 0.15 AOT. The derived results are compared against the input values. The results show that the M3/M5 ratio has bias of −0.008–0.005 and RMSE of 0.001–0.008 due to the

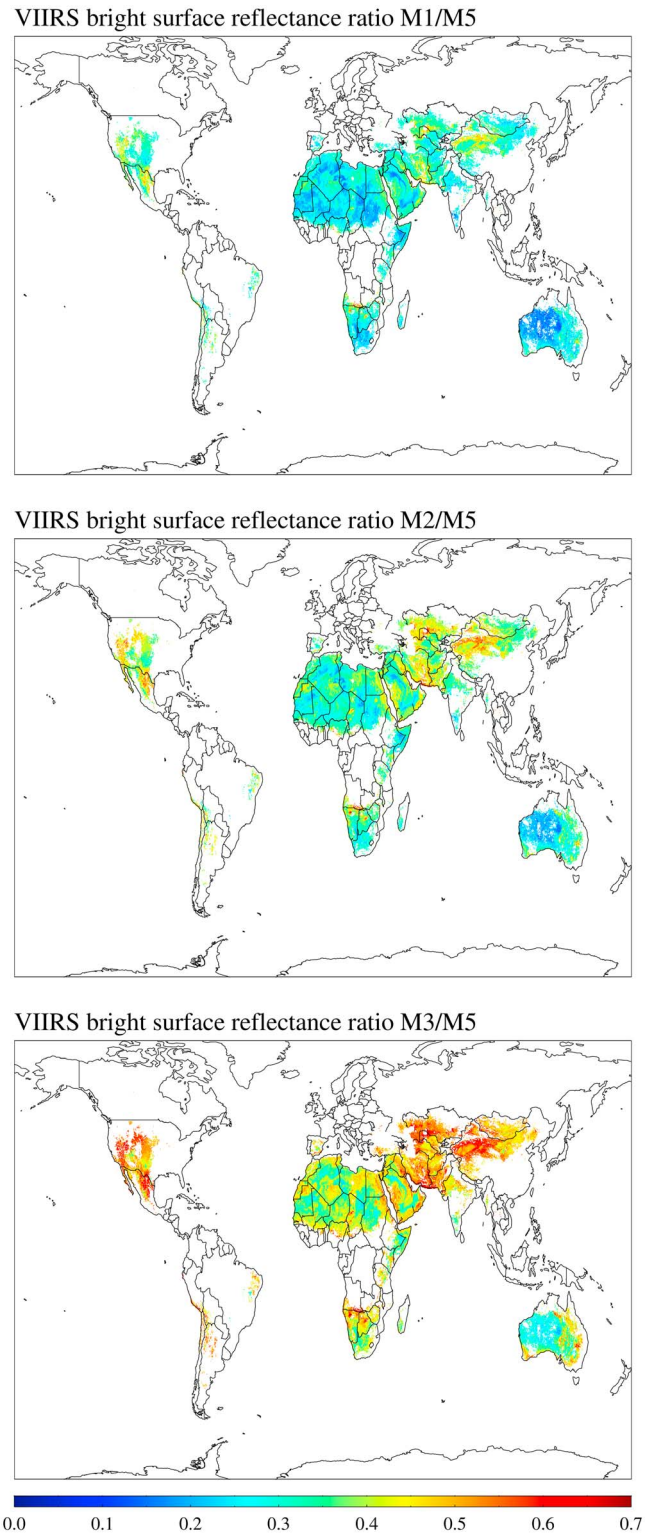

Figure 8. Surface reflectance ratios for bright pixels (backward reflectantion geometry with scattering angle 140°).

wrong aerosol models used. The M1/M5 ratio has bias of −0.011–0.012 and RMSE of 0.002–0.013. The uncertainties are small compared to the standard deviation of the ratios at this site (Table 5). They are much less than the differences between the ratios in Table 5 and those used in the operational algorithm at Solar Village, which are 0.204 for M1/M5 and 0.185 for M3/M5.

The derived database contains the linear regression coefficients of the lower bounds of the atmospherically corrected reflectance ratios for the forward and the backward reflection geometries. The ratios include M1/M5, M2/M5, and M3/M5 for both types of pixels, and M5/M11 for the dark pixels only.

Figure 8 shows the global map of the derived surface reflectance ratios at a selected geometry for M1/M5, M2/M5, and M3/M5 for the bright pixels. The geometry is backward reflection with a scattering angle of 140° for each 0.1°×0.1° grid box. As shown in Figure 8, the bright pixels are mostly distributed over the regions of Africa, western Asia, northwest China, Australia, and western continental U.S. The regions of bright pixels are larger in the backward reflection geometries than those in the forward reflection geometries (not shown here). This is because the surface reflectances are generally higher in the backward reflection geometries than those in the forward reflection geometries. The bright pixels with the M11 TOA reflectances close to 0.25 in the backward reflection geometries may have M11 TOA reflectance lower than 0.25 in the forward reflection geometries. Consequently, the number of bright pixels is less in the forward geometries.

Figure 8 also demonstrates that the surface reflectance ratios change from region to region. For example, the M3/M5 ratio has a range between 0.3 and 0.7: the area with the lowest M3/M5 ratio is in Australia; that with the highest is in the northwest China and Mexico. Even within the same region, the ratios also vary from one grid box to another. Such observation further confirms our statement that we need a surface reflectance ratio database for an improved AOT

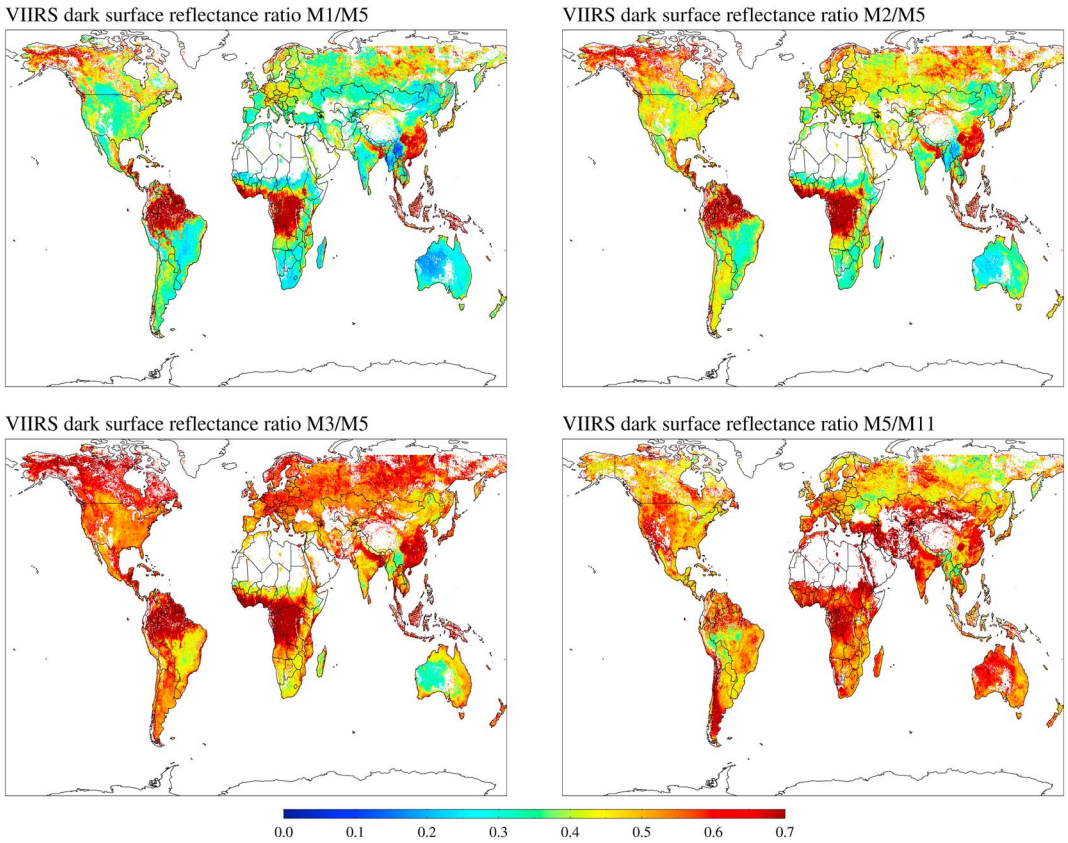

Figure 9. Surface reflectance ratios for dark pixels (backward reflection geometry with scattering angle 140°).

retrieval algorithm. Many bright surfaces have significantly lower ratios than the ones used in the operational dark pixel AOT retrieval algorithm shown in Table 2.

Similarly, Figure 9 plots the surface reflectance ratios for dark pixels with the same geometries as Figure 8. Again, the surface reflectance ratios vary from region to region. The smallest ratios for M3/M5 are found in Australia with values around 0.3, while the current operational model uses a single value of 0.645 over the entire globe and therefore tends to significantly underestimate or retrieve negative AOT in those areas.

6. AOT Retrieval Algorithm Over Land Using the Surface Reflectance Ratio Database

The AOT retrieval algorithm over land using the derived surface ratio database is an enhancement of the algorithm of the current operational AOT retrieval algorithm [*Jackson et al*., 2013], described in section 3.

The enhanced algorithm is modified from the algorithm described in section 3 in the following ways: The enhanced algorithm not only works over dark surfaces but also works over bright surfaces. Within the algorithm, instead of fixed ratios, the surface reflectance ratio R_n between band Mn and band M5 for a pixel is obtained from the global $0.1° \times 0.1°$ surface reflectance ratio database through spatial interpolation using the four closest boxes. The use of spatial interpolation is to allow the surface reflectance ratios to change smoothly from one $0.1° \times 0.1°$ box to the adjacent one. Otherwise, the boundaries between the grid boxes will show up in the final retrieved AOT map. The surface reflectance ratios of a particular VIIRS pixel are obtained from the database of either dark surface or bright surface depending on the classification of the pixel, i.e., a pixel is dark if its M11 TOA reflectance is less than 0.25 and vise versa.

Besides the surface reflectance ratios, the retrieval algorithm over dark pixels does not have any additional change from the current operational algorithm. For bright pixels, however, we change the selection of the aerosol models and the bands to retrieve AOT. Although we make the aerosol model selection in the algorithm, we found that the algorithm's ability to choose the correct aerosol model is of dubious benefit,

Table 9. Statistics of VIIRS AOT Retrieval Over Bright Surfaces Using Different Surface Reflectance Ratios Compared Against AERONET AOT

	Surface Reflectance Ratio Used for AOT Retrieval	*R*	Mean Bias	STD of Error	RMSE	Slope	Intercept	*N*
North Africa and Arabian Peninsula	M1/M5	0.67	−0.113	0.175	0.208	0.42	0.06	4518
	M2/M5	0.77	−0.077	0.149	0.168	0.59	0.05	4503
	M3/M5	0.80	−0.031	0.141	0.145	0.71	0.06	4482
Regions other than North Africa and Arabian Peninsula	M1/M5	0.60	0.044	0.125	0.132	0.49	0.10	2655
	M2/M5	0.60	0.060	0.122	0.136	0.56	0.11	2604
	M3/M5	0.55	0.097	0.136	0.167	0.59	0.14	2522

especially when dust occurs over high surface reflectance regions. Therefore, for North Africa and the Arabian Peninsula region (latitude in [0°,36°N] and longitude in [20°W,60°E]), instead of choosing the aerosol model in the algorithm, we forcibly set the aerosol model to dust; i.e., the loop over aerosol models is not executed in the algorithm for this region. As discussed in section 4, we do not use M11 in calculation of the residuals for aerosol model selection over bright surfaces.

We still use the M3 and M5 pair to retrieve AOT on the bright surfaces over North Africa and Arabian Peninsula region. But we use the M1 and M5 pair to retrieve AOT for the other bright surface regions. The band pair for AOT retrieval over bright surface is based on the evaluation of the AOT retrieval accuracy with different pairs at AERONET. The use of M3 and M5 pair over North Africa and Arabian Peninsula and the use of M1 and M5 pair over the other regions provide better AOT retrievals than those using the other band pairs, as demonstrated in Table 9.

Most of the quality control criteria are the same as those in the VIIRS operational AOT retrieval algorithm. There are some differences in the quality controls of the pixels between this work and the ones in *Godin* [2015]. These modifications are shown in Table 10.

7. Results

7.1. Comparison Against AERONET AOT

To validate the AOT retrieval algorithm using the surface reflectance ratio database, we compare the enhanced VIIRS AOT retrieval results against AERONET AOT observations. VIIRS AOT is retrieved for each VIIRS pixel, and therefore, it has a spatial resolution of 750 m at nadir. We perform the AOT retrieval using the 2 year (May 2012 to April 2014) data set of matchups between VIIRS and AERONET. The matchup criteria are (1) at least two AERONET AOT measurements within ±30 min of the satellite overpass and (2) at least 800 pixels of high-quality VIIRS AOT retrievals within the 27.5 km area surrounding the AERONET site, which is about 20% of all the pixels in this area at nadir.

Figure 10 shows the scatterplots of the comparison of high-quality VIIRS AOT retrievals against AERONET AOT. The results for bright surfaces and for dark surfaces are evaluated separately in Figures 10a and 10b, respectively. To demonstrate the improvement over AOT from the currently operational algorithm, we also show the scatterplot of VIIRS AOT using the original surface reflectance ratios versus AERONET AOT in Figure 10c. To make fair comparison, VIIRS AOT retrievals in Figure 10c are the reprocessed results using the updated code and LUT, except for using the original surface reflectance ratios.

The total number of matchups over bright surfaces of the VIIRS AOT and AERONET AOT is 6937. These are retrievals that would not be possible using the operational dark target algorithm. The AOT retrievals over

Table 10. Quality Control Criteria Revisions in This Work, Where the Central Wavelengths for Bands M7, M8, and M15 are 0.865 μm, 1.24 μm, and 10.763 μm

Test Names	Details
AOT range	[−0.05, 5.0]
Bright surface	If TOA reflectance of M11 > 0.25, then use retrieval algorithm over bright surface.
Ephemeral water	Removed
Snow ice test	(M7 − M8)/(M7 + M8) > 0.01 and brightness temperature of M15 < 285

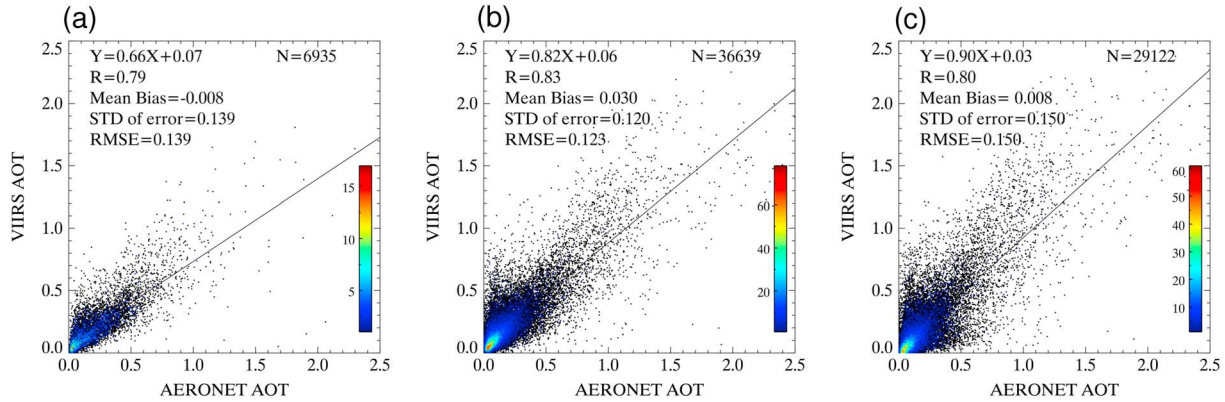

Figure 10. Scatterplots of the AERONET AOT and VIIRS AOT over global AERONET sites: (a) bright pixels; (b) dark pixels using the new surface reflectance ratios; (c) dark pixels using the original surface reflectance ratios.

the bright surfaces have a correlation coefficient of 0.79 against AERONET AOT, a mean bias of −0.008, a standard deviation of error of 0.139, and an RMSE of 0.139. The sites with bright pixels are mostly located in North Africa, the Arabian Peninsula, and the western United States regions.

Over dark surfaces, the VIIRS AOT retrievals using the revised surface reflectance ratios have improved the standard deviation of error, RMSE, and total number of the matchups: The RMSE improves from 0.150 to 0.123. The total number of matchups increased more than 26%. However, the mean bias is worse than before, as is the regression slope. Since the only difference in the retrieval algorithms used to produce the data in Figures 10b and 10c is the surface reflectance ratios, we can conclude that the changes in the AOT retrieval over the dark surfaces is due to the use of different surface reflectance ratios.

To further compare the AOT retrieval from this work and those from the current operational algorithm, we show scatter plots of VIIRS AOT versus AERONET AOT that have one-to-one correspondence between the two algorithms in Figure 11. Those additional retrievals in Figure 10b are removed. These plots also show that the algorithm using the surface reflectance ratio database has improved standard deviation of error and RMSE over the current operational algorithm. However, the mean bias is higher in the AOT retrievals using the updated ratios.

To compare the enhanced VIIRS AOT retrieval with the MODIS Deep Blue AOT over the bright surfaces, we plot in Figure 12 the scatter plots of VIIRS AOT versus AERONET AOT and MODIS Deep Blue AOT versus AERONET AOT for AERONET stations in the North Africa and Arabian Peninsula region. The MODIS Deep Blue algorithm retrieves AOT from MODIS visible bands over bright surfaces using a 0.1° × 0.1° spatial resolution surface reflectance database at a spatial resolution of 10 km at nadir [*Sayer et al.*, 2013]. Similar to the

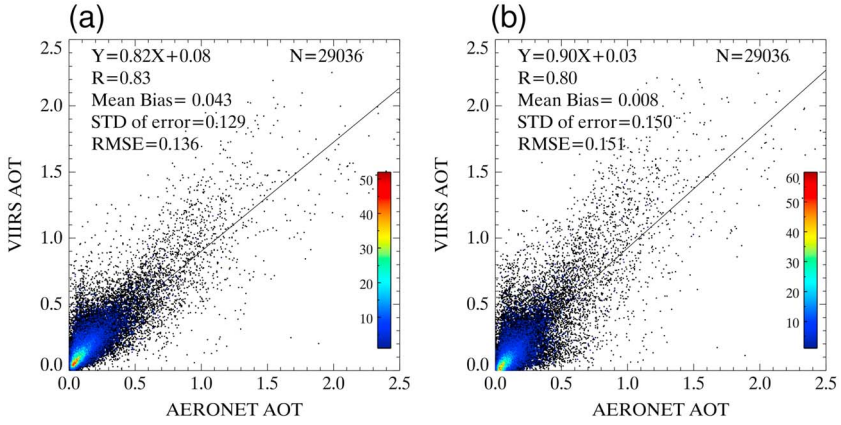

Figure 11. Scatterplots of VIIRS AOT versus AERONET AOT with one-to-one correspondence between (a) this work and (b) the current operational algorithm over the dark surfaces.

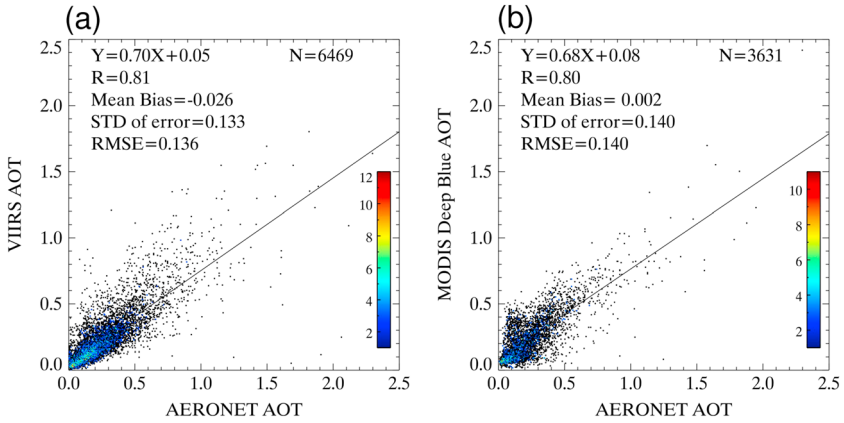

Figure 12. Scatterplots of AOT over North Africa and Arabian Peninsula region: (a) VIIRS AOT versus AERONET AOT; (b) MODIS Deep Blue AOT versus AERONET AOT.

matchup criteria between VIIRS AOT and AERONET AOT, we require that MODIS Deep Blue AOT have at least five high-quality retrievals within the 27.5 km circle surrounding the AERONET site in order to be counted, i.e., more than 20% of possible 10 km retrievals. Since MODIS Deep Blue AOT does not differentiate bright pixels from dark pixels, to make the comparison fair, in the scatterplots of Figure 12, we include AOT retrievals at both VIIRS dark and bright pixels for the matchup. We can see from the scatterplots that the VIIRS AOT shows a slight advantage in terms of standard deviation of error, but overall, the retrievals have similar performance in terms of validation statistics. However, the total number of the matchup between MODIS and AERONET AOT is much less than that between VIIRS and AERONET AOT: the VIIRS swath is 30% wider than MODIS's swath, but the total number of the matchup is 78% more. The MODIS Deep Blue AOT retrieval algorithm therefore likely enforces stricter quality controls and removes more AOT retrievals.

7.2. Examples of Regional Aerosol Events

We demonstrate the performance of the regional AOT retrieval by running the AOT retrieval algorithm for two examples: one is over North Africa and the Arabian Peninsula, the other is over the western United States.

The North Africa and Arabian Peninsula region is mostly covered by desert, and therefore, the surface reflectances in the region are high. For example, as shown in Figure 2, the surface reflectances of VIIRS pixels close to the Solar Village site are between 0.3 and 0.4 in the M5 channel and are between 0.3 and 0.5 in the M11 channel. Since the current operational VIIRS AOT retrieval algorithm only retrieves AOT over dark surfaces, it does not retrieve AOT in this region. Figure 13 shows the VIIRS RGB and AOT retrieval plots for 23 August 2013. The MODIS Deep Blue AOT retrieval is also plotted for comparison. A visual inspection of the RGB image indicates several big dust storms at different places over this region. Both VIIRS and MODIS Deep Blue algorithm retrieve high AOT in south Algeria, north Mali, Mauritania, and the middle Niger. The areas of low AOT regions are mostly similar. Therefore, the AOT retrieval patterns over this region are qualitatively the same between the enhanced VIIRS AOT retrieval and the MODIS Deep Blue AOT retrievals. However, we also noticed three differences between the VIIRS and the MODIS Deep Blue AOT retrievals: (1) high AOT retrievals in the VIIRS retrieval over Sudan are not observed in the MODIS Deep Blue AOT retrievals; (2) the MODIS deep blue retrieval hints at high AOT over southern Algeria but is missing the highest values where VIIRS reports AOT greater than 2.0; and (3) VIIRS AOT retrieval has more extensive coverage over some regions such as the Arabian Peninsula and regions along the north coast of Africa. These differences may be caused by the difference in the screening algorithms between the enhanced VIIRS and the MODIS Deep Blue algorithm, which we also noticed in the AERONET AOT matchup in the last subsection. However, without ground observation in these areas, it is hard to tell whether VIIRS is being foolhardy in its expansive coverage or whether MODIS deep blue is too conservative.

Figure 14 shows a comparison between 16 day average VIIRS AOT and Multiangle Imaging Spectroradiometer (MISR) AOT over North Africa and Arabian Peninsula. Since MISR only has a swath width of 360 km, it cannot cover the whole area in 1 day. Therefore, we average AOT over a 16 day period so that it covers the whole

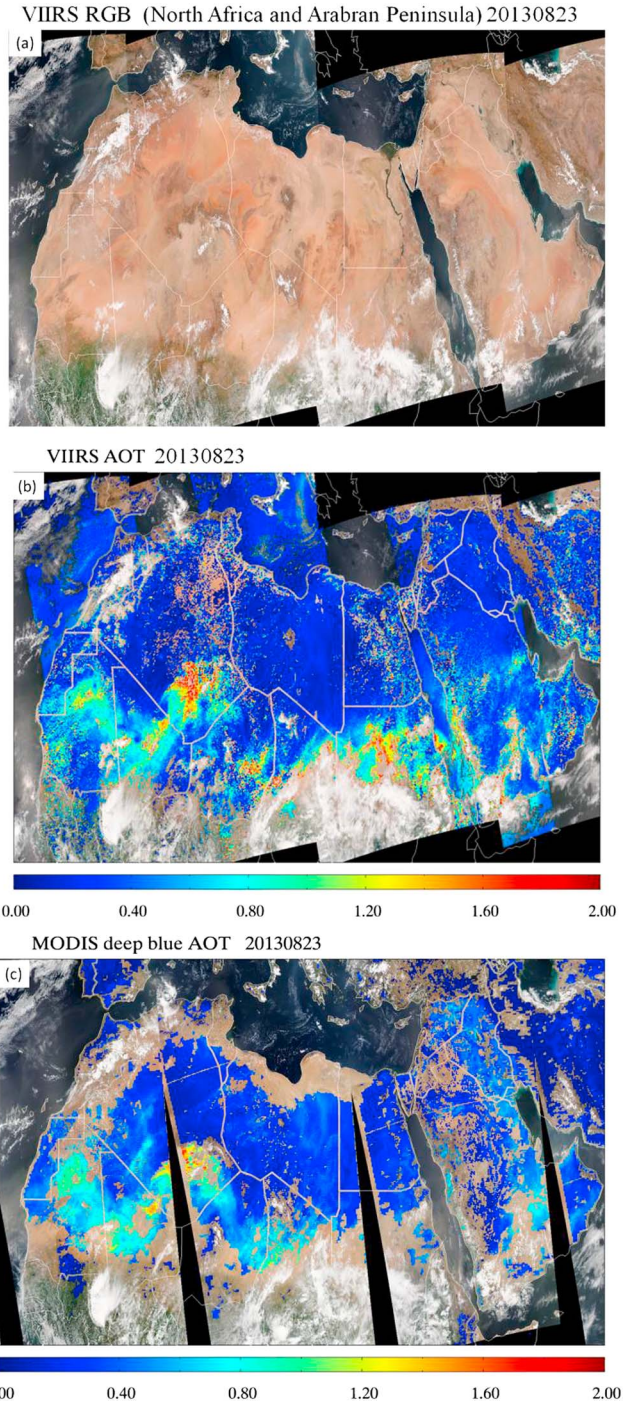

Figure 13. Regional retrieval over bright surfaces: North Africa and Arabian Peninsula region on 23 August 2013. (a) VIIRS RGB true-color image; (b) VIIRS AOT retrieval using the surface reflectance ratio database; (c) MODIS Deep Blue high quality AOT.

area. The VIIRS AOT is regridded into a 0.25°×0.25° grid and MISR AOT is into a 0.5°×0.5° grid. We only use the VIIRS AOT in the grids that MISR also have values so that both of them cover the same area. However, because the two sensors have different overpass times, we do not expect them to compare well pixel by pixel. The mean AOT patterns from the two sensors agree well in most of the region, which indicates that both sensors catch the same events during this period. Some of the high AOT regions found in both images are in Southern Algeria, Northern Mali, in the middle of Niger, Western Chad, and Northern Sudan.

Figure 15 shows a smoke case study over the western United States on 9 September 2014, where we compare the AOT retrievals from the algorithm in this work (Figure 15b) and the reprocessed high-quality AOT using the current operational algorithm (Figure 15c). The difference between AOT retrieval algorithms are the surface reflectance ratios used and the quality controls from the surface types. In Figure 15b, we retrieve over all types of surfaces. In Figure 15c, we retrieve only dark target pixels. The surfaces over the western United States are complicated: they contain both dark pixels and bright pixels. Some areas are dark even though they are dominated by soil. Those soil-dominated regions usually have surface reflectance ratios M3/M5 less than the one used in the current operational VIIRS AOT retrieval algorithm. The use of an M3/M5 ratio higher than the real ratio can reduce the retrieved AOT values. Therefore, the current operational algorithm marked soil-dominated pixels as "degraded" quality. In Figure 15c, most cloud-free areas without AOT retrievals are soil-dominated regions, which are marked as degraded in the current operational algorithm. Especially, the smoke plumes in northwestern Nevada are not shown in the AOT retrievals from the current operational VIIRS algorithm. The enhanced algorithm using the surface reflectance ratio database solved this problem. As shown in Figure 15b, most of the AOT retrieval gaps are filled with AOT retrievals. We also observe differences in the retrieved AOT values between the two algorithms. For example, the retrievals from the enhanced algorithm have an AOT streak close to 1.0, which is down the center of the plume that

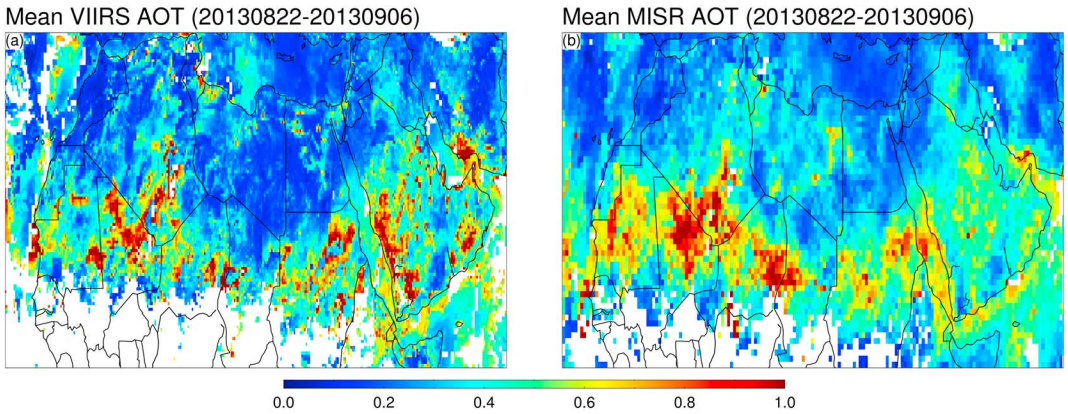

Figure 14. Sixteen day average AOT over North Africa and the Arabian Peninsula: (a) VIIRS AOT; (b) MISR AOT.

crosses California to the ocean. The AOT retrievals of the operational algorithm have much lower values for this plume. This is also caused by the differences in the surface reflectance ratios used in the algorithm.

The two examples in this section demonstrate that the use of the surface reflectance ratio database for AOT retrieval can improve data coverage of the VIIRS AOT retrievals. The additional data coverage regions are mostly located either in the bright surface regions or the soil-dominated surface regions.

8. Discussions and Conclusions

In this paper, we developed a global surface reflectance ratio database with a spatial resolution of $0.1° \times 0.1°$ based on the 2 years of VIIRS observations (May 2012 to April 2014). The database contains the surface reflectance ratios of M1/M5, M2/M5, and M3/M5 for both dark and bright surfaces and M5/M11 for dark surfaces. Using the global surface reflectance ratio database, we enhanced the VIIRS AOT retrieval algorithm over land such that it is able to retrieve AOT over both dark and bright surfaces. Compared to AERONET AOT, the VIIRS AOT retrievals from the enhanced algorithm have improved RMSE over the dark surfaces over those from the current operational AOT retrieval algorithm. The enhanced AOT retrieval algorithm also extends the AOT retrieval data coverage to bright surfaces and dark surfaces dominated by soil, where the current operational AOT retrieval algorithm does not work or does not work well. The enhanced VIIRS AOT retrievals compare well with AERONET AOT and MODIS Deep Blue AOT. The enhanced VIIRS AOT also greatly improved the AOT retrieval data coverage over both dark and bright surfaces.

The surface reflectance ratio database is created from the atmospheric correction of measured VIIRS TOA reflectances across the $0.1° \times 0.1°$ grid. The atmospheric correction takes into account Rayleigh scattering, gaseous absorption, and a background aerosol loading. Background aerosol loading is determined from finding the lowest envelope AOT value at AERONET stations and then interpolating this value across the global grid. Mostly, background AOT is negligible and assumptions concerning interpolation between AEROSOL stations or aerosol type for the atmospheric correction calculation matter little. However, in some regions, background AOT can be as high as 0.15, and then interpolation and aerosol assumptions introduce uncertainty into the final product. There is some concern in regions with nonnegligible background aerosol loading that comparison with AERONET will overestimate the validity of the method because the retrievals will always be best at the AERONET station locations where the formulation data are obtained, in contrast with points requiring interpolation from stations that may be hundreds or thousands of kilometers distant.

The algorithm is based on two assumptions. The first is that two sets of surface reflectance ratios are applicable across the $0.1° \times 0.1°$ grid square, one for bright pixels and the other for dark pixels, and the second is that there is no seasonality in surface conditions or in aerosol type when significant background AOT exists. The first assumption was tested at two AERONET sites: Solar Village and Banizoumbou. At these two sites, the variability in surface reflectance ratio within a 10 km area ranges from 5% to 30% of the mean, depending on site and the choice of bands used in the ratio. This uncertainty in ratio introduces an uncertainty in AOT retrieval of 18% to 32%, depending on site. The effects of the second assumption of no significant seasonality have not yet been tested.

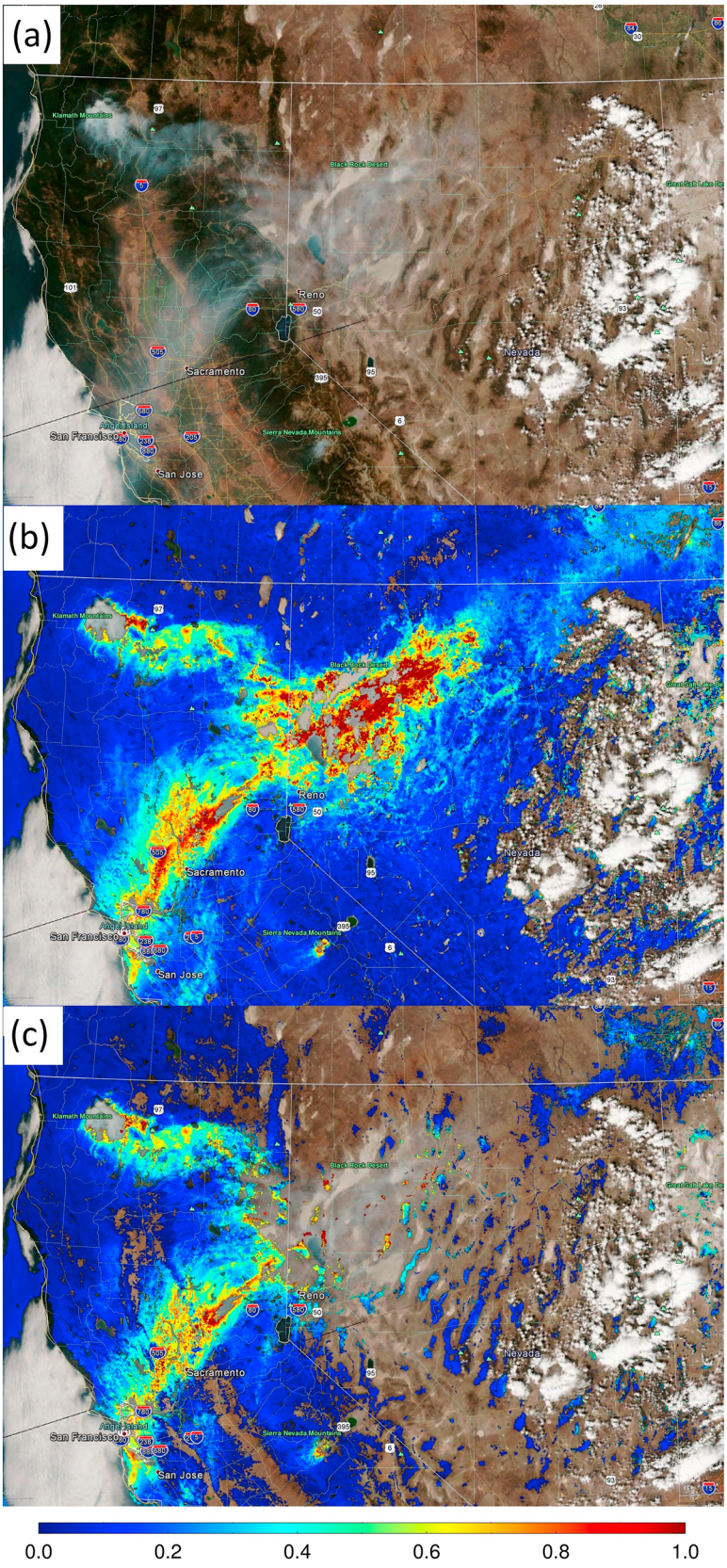

Figure 15. Smoke over the western United States on 9 September 2014. (a) VIIRS RGB image; (b) VIIRS AOT retrieval using the surface reflectance ratios database; (c) VIIRS high quality IP AOT retrievals from current operational dark target algorithm.

In the future, we will further improve the accuracy in the estimated surface reflectance ratios by introducing seasonality to the database. This will be of greater importance over dark surfaces than bright surfaces because of the seasonal change in the color of vegetation over an annual cycle. Therefore, even at the same location, we have to use different surface reflectance ratios in different seasons. One potential solution is to investigate the dependence of the ratios on NDVI for the dark surfaces and develop empirical equations to model such seasonal variations, similar to what is used in the MODIS dark target algorithm [*Levy et al*., 2007b]. Another solution is to build different surface reflectance ratio databases for different seasons when we have many years of VIIRS data available.

For now, especially over truly bright barren surfaces, the algorithm presented above does indeed retrieve AOT that meets validation criteria on an annual and global basis. In addition, the algorithm offers quantitative aerosol loading information for case studies of important aerosol events.

Acknowledgments
This work is supported by the NOAA JPSS program. The authors thank the MODIS team and AERONET principal investigators and site managers for providing the data used in this work. The contents in this paper are solely the opinions of the authors and do not constitute a statement of policy, decision, or position on behalf of NOAA or the U.S. Government. The data used in this paper can be requested from Istvan Laszlo (Istvan.Laszlo@noaa.gov) or Shobha Kondragunta (Shobha.Kondragunta@noaa.gov).

References

Al-Saadi, J., et al. (2005), Improving national air quality forecasts with satellite aerosol observations, *Bull. Am. Meteorol. Soc.*, *86*, 1249–1264, doi:10.1175/BAMS-86-9-1249.

Bellouin, N., O. Boucher, J. Haywood, and M. S. Reddy (2005), Global estimate of aerosol direct radiative forcing from satellite measurements, *Nature*, *438*, 1138–1141, doi:10.1038/nature04348.

Cao, C. (2013a), Joint Polar Satellite System (JPSS) Visible Infrared Imaging Radiometer Suite (VIIRS) Sensor Data Records (SDR) Algorithm Theoretical Basis Document (ATBD), E/RA-00003, Rev. C.

Cao, C. (2013b), Joint Polar Satellite System (JPSS) Visible Infrared Imaging Radiometer Suite (VIIRS) Sensor Data Records (SDR) Geolocation Algorithm Theorecical Basis Document (ATBD), E/RA-00004, Rev. A.

Cavalieri, O., et al. (2010), Variability of aerosol vertical distribution in the Sahel, *Atmos. Chem. Phys.*, *10*, 12,005–12,023, doi:10.5194/acp-10-12005-2010.

Chin, M., et al. (2014), Multi-decadal variations of atmospheric aerosols from 1980 to 2009: A perspective from observations and a global model, *Atmos. Chem. Phys.*, *14*, 3657–3690.

de Leeuw, G., et al. (2015), Evaluation of seven European aerosol optical depth retrieval algorithms for climate analysis, *Remote Sens. Environ.*, *162*, 295–315, doi:10.1016/j.rse.2013.04.023.

Dubovik, O., B. Holben, T. F. Eck, A. Smirnov, Y. J. Kaufman, M. D. King, D. Tanré, and I. Slutsker (2002), Variability of absorption and optical properties of key aerosol types observed in worldwide locations, *J. Atmos. Sci.*, *59*, 590–608, doi:10.1175/1520-0469(2002)059<0590:VOAAOP>2.0.CO;2.

Engel-Cox, J. A., C. H. Holloman, B. W. Coutant, and R. M. Hoff (2004), Qualitative and quantitative evaluation of MODIS satellite sensor data for regional and urban scale air quality, *Atmos. Environ.*, *38*, 2495–2509, doi:10.1016/j.atmosenv.2004.01.039.

Fraser, R. S., and Y. J. Kaufman (1985), The relative importance of aerosol scattering and absorption in remote sensing, *IEEE Trans. Geosci. Remote Sens.*, *GE23*, 625–633.

Godin, R. (2014), Joint Polar Satellite System (JPSS) VIIRS Cloud Mask (VCM) Algorithm Theoretical Basis Document (ATBD), Joint Polar Satellite System (JPSS) Ground Project Code 474, 474-00033, GSFC JPSS CMO, December 9, 2014 released.

Godin, R. (2015), Joint Polar Satellite System (JPSS) VIIRS Aerosol Optical Thickness (AOT) and Particle Size Parameter Algorithm Theoretical Basis Document (ATBD), Joint Polar Satellite System (JPSS) Ground Project Code 474, 474-00049, GSFC JPSS CMO, April 2, 2015 released.

Hoff, R. M., et al. (2009), Applications of the three-dimensional air quality system to western U.S. air quality: IDEA, smog blog, smog stories, AirQuest, and the remote sensing information gateway, *J. Air Waste Manage.*, *59*(8), 980–989, doi:10.3155/1047-3289.59.8.980.

Holben, B. N., et al. (1998), AERONET—A federated instrument network and data archive for aerosol characterization, *Remote Sens. Environ.*, *66*, 1–16, doi:10.1016/S0034-4257(98)00031-5.

Hsu, N. C., S. C. Tsay, M. D. King, and J. R. Herman (2004), Aerosol properties over bright-reflecting source regions, *IEEE Trans. Geosci. Remote Sens.*, *42*, 557–569, doi:10.1109/TGRS.2004.824067.

Hsu, N. C., S. C. Tsay, M. D. King, and J. R. Herman (2006), Deep blue retrievals of Asian aerosol properties during ACE-Asia, *IEEE Trans. Geosci. Remote Sens.*, *44*, 3180–3195, doi:10.1109/TGRS.2006.879540.

Hsu, N. C., M.-J. Jeong, C. Bettenhausen, A. M. Sayer, R. Hansell, C. S. Seftor, J. Huang, and S.-C. Tsay (2013), Enhanced Deep Blue aerosol retrieval algorithm: The second generation, *J. Geophys. Res. Atmos.*, *118*, 9296–9315, doi:10.1002/jgrd.50712.

Isaaks, E. H., and R. M. Srivastava (1989), *Applied Geostatistics*, Oxford Univ. Press, New York.

Jackson, J. M., H. Liu, I. Laszlo, S. Kondragunta, L. A. Remer, J. Huang, and H.-C. Huang (2013), Suomi-NPP VIIRS aerosol algorithms and data products, *J. Geophys. Res. Atmos.*, *118*, 12,673–12,689, doi:10.1002/2013JD020449.

Kahn, R. A., B. J. Gaitley, M. J. Garay, D. J. Diner, T. F. Eck, A. Smirnov, and B. N. Holben (2010), Multiangle Imaging SpectroRadiometer global aerosol product assessment by comparison with the Aerosol Robotic Network, *J. Geophys. Res.*, *115*, D23209, doi:10.1029/2010JD014601.

Kahn, R., B. Gaitley, J. Martonchik, D. Diner, K. Crean, and B. Holben (2005), Multiangle Imaging Spectroradiometer (MISR) global aerosol optical depth validation based on two years of coincident Aerosol Robotic Network (AERONET) observations, *J. Geophys. Res.*, *110*, D10S04, doi:10.1029/2004JD004706.

Kaufman, Y. J. (1987), Satellite sensing of aerosol absorption, *J. Geophys. Res.*, *92*(D4), 4307–4317, doi:10.1029/JD092iD04p04307.

Kaufman, Y. J., D. Tanré, L. A. Remer, E. F. Vermote, A. Chu, and B. N. Holben (1997a), Operational remote sensing of tropospheric aerosol over land from EOS moderate resolution imaging spectroradiometer, *J. Geophys. Res.*, *102*(D14), 17,051–17,067, doi:10.1029/96JD03988.

Kaufman, Y. J., A. E. Wald, L. A. Remer, B.-C. Gao, R.-R. Li, and L. Flynn (1997b), The MODIS 2.1-μm channel-correlation with visible reflectance for use in remote sensing of aerosol, *IEEE Trans. Geosci. Remote Sens.*, *35*, 1286–1296, doi:10.1109/36.628795.

Kaufman, Y. J., D. Tanré, and O. Boucher (2002), A satellite view of aerosols in the climate system, *Nature*, *419*, 215–223, doi:10.1038/nature01091.

Kotchenova, S. Y., and E. F. Vermote (2007), Validation of a vector version of the 6S radiative transfer code for atmospheric correction of satellite data. Part II: Homogeneous Lambertian and anisotropic surfaces, *Appl. Opt.*, *46*, 4455–4464.

Kotchenova, S. Y., E. F. Vermote, R. Matarrese, and F. J. Klemm Jr. (2006), Validation of a vector version of the 6S radiative transfer code for atmospheric correction of satellite data. Part I: Path radiance, *Appl. Opt.*, *45*, 6762–6774.

Levy, R. C., L. A. Remer, and O. Dubovik (2007a), Global aerosol optical properties and application to Moderate Resolution Imaging Spectroradiometer aerosol retrieval over land, *J. Geophys. Res.*, *112*, D13210, doi:10.1029/2006JD007815.

Levy, R. C., L. A. Remer, S. Mattoo, E. F. Vermote, and Y. J. Kaufman (2007b), Second-generation operational algorithm: Retrieval of aerosol properties over land from inversion of Moderate Resolution Imaging Spectroradiometer spectral reflectance, *J. Geophys. Res.*, *112*, D13211, doi:10.1029/2006JD007811.

Levy, R. C., L. A. Remer, R. G. Kleidman, S. Mattoo, C. Ichoku, R. Kahn, and T. F. Eck (2010), Global evaluation of the Collection 5 MODIS dark-target aerosol products over land, *Atmos. Chem. Phys.*, *10*, 10,399–10,420, doi:10.5194/acp-10-10399-2010.

Liu, H., L. A. Remer, J. Huang, H.-C. Huang, S. Kondragunta, I. Laszlo, M. Oo, and J. M. Jackson (2014), Preliminary evaluation of S-NPP VIIRS aerosol optical thickness, *J. Geophys. Res. Atmos.*, *119*, 3942–3962, doi:10.1002/2013JD020360.

Lucht, W., C. B. Schaaf, and A. H. Strahler (2000), An algorithm for the retrieval of albedo from space using semiempirical BRDF models, *IEEE Trans. Geosci. Remote Sens.*, *38*, 977–998, doi:10.1109/36.841980.

Popp, T., et al. (2016), Development, production and evaluation of aerosol Climate Data Records from European satellite observations (Aerosol_cci), *Remote Sens.*, *8*, 421, doi:10.3390/rs8050421.

Prados, A. I., S. Kondragunta, P. Ciren, and K. R. Knapp (2007), GOES Aerosol/Smoke Product (GASP) over North America: Comparisons to AERONET and MODIS observations, *J. Geophys. Res.*, *112*, D15201, doi:10.1029/2006JD007968.

Quaas, J., O. Boucher, N. Bellouin, and S. Kinne (2008), Satellite-based estimate of the direct and indirect aerosol climate forcing, *J. Geophys. Res.*, *113*, D05204, doi:10.1029/2007JD008962.

Remer, L. A., A. E. Wald, and Y. J. Kaufman (2001), Angular and seasonal variation of spectral surface reflectance ratios: Implications for the remote sensing of aerosol over land, *IEEE Trans. Geosci. Remote Sens.*, *39*(2), 275–283, doi:10.1109/36.905235.

Sayer, A. M., N. C. Hsu, C. Bettenhausen, and M.-J. Jeong (2013), Validation and uncertainty estimates for MODIS Collection 6 "Deep Blue" aerosol data, *J. Geophys. Res. Atmos.*, *118*, 7864–7872, doi:10.1002/jgrd.50600.

Schowengerdt, R. A. (1983), *Techniques for Image Processing and Classifications in Remote Sensing*, Academic Press Inc., New York.

Torres, O., A. Tanskanen, B. Veihelmann, C. Ahn, R. Braak, P. K. Bhartia, P. Veefkind, and P. Levelt (2007), Aerosols and surface UV products from Ozone Monitoring Instrument observations: An overview, *J. Geophys. Res.*, *112*, D24S47, doi:10.1029/2007JD008809.

van Donkelaar, A., R. V. Martin, M. Brauer, R. Kahn, R. Levy, C. Verduzco, and P. J. Villeneuve (2010), Global estimates of ambient fine particulate matter concentrations from satellite-based aerosol optical depth: Development and application, *Environ. Health Perspect.*, *118*(6), 847–55, doi:10.1289/ehp.0901623.

van Donkelaar, A., R. V. Martin, M. Brauer, N. C. Hsu, R. A. Kahn, R. C. Levy, A. Lyapustin, A. M. Sayer, and D. M. Winker (2016), Global estimates of fine particulate matter using a combined geophysical-statistical method with information from satellites, models, and monitors, *Environ. Sci. Technol.*, *50*(7), 3762–3772, doi:10.1021/acs.est.5b05833.

Vermote, E. F., D. Tanré, J. L. Deuzé, M. Herman, and J.-J. Morcrette (1997), Second simulation of the satellite signal in the solar spectrum, 6S: An overview, *IEEE Trans. Geosci. Remote Sens.*, *35*, 675–686.